Aalto University
School of Engineering

Xi Fan

3D Scanning and Computer-aided Tolerance Software Analysis for Product Inspection

Thesis submitted in partial fulfillment of the requirements for the degree of Master of Science in Technology

Espoo, November 30, 2018
Supervisor: Professor Kevin Otto
Advisor: Rurik Englund

Aalto University
School of Engineering

Aalto University, P.O. BOX 11000, 00076 AALTO

www.aalto.fi

Abstract of master's thesis

Author Xi Fan		
Title of thesis 3D Scanning and Computer-aided tolerance software analysis for product inspection		
Master programme Mechanical Engineering		**Code** ENG25
Thesis supervisor Professor Kevin Otto		
Thesis advisor Rurik Englund		
Date 30.11.2018	**Number of pages** 61+9	**Language** English

Abstract

Tolerances are vital for every physical product, with a tight connection and competing needs between engineering design and manufacturing. 1D, 2D and 3D tolerance analysis can be applied to any product for determining these tolerances. With increase in dimensions the difficulty of tolerance analysis also increases. This research explores tolerance analysis in 3D situation.

3D scanning is a recently developed technology. In the industrial field, this technology is popular for inspecting product quality and in reverse engineering. It compares the dimensions between the 3D scanning model and the CAD model to inspect product quality. It also can generate a CAD model out of the 3D scanning model used in reverse engineering. The device mainly used in 3D scanning is the 3D optical scanner and the 3D laser scanner. These two types of 3D scanner use the same triangulation principle but one uses optical light and the other laser light.

This research includes a 3D tolerance analysis and 3D scan. Before tolerance analysis a tolerance stack-up analysis was completed. Tolerance analysis was done using Crystal Ball software. The software uses Monte Carlo simulation to get results based on HTM calculator in Excel. HTM calculator contains every transformation nominal position and tolerance value. HTM calculated nominal position distance should be the same as CAD software Creo measured distance. Transformation nominal position was based on a loop diagram. Tolerance value was based on the defined tolerance in drawing and 3D scanning value. 3D scanning in this research is used to inspect product quality. Both parts and the assembly device were scanned. Parts were selected based on the loop diagram. The device was assembled using 3D scanning parts.

The results of the tolerance analysis were shown through distribution charts and sensitivity charts. Comparing the simulation results of 3D scanning data and defined tolerances in drawing, distribution charts results were not reliable but sensitivity charts results were similar. The results of 3D scanning measurement data show the current device tolerance value is too tight. 3D scanning devices used in this research are not suited for large scale implementation, e.g. in product inspection.

Keywords 3D Scanning, tolerance analysis, HTM, Monte Carlo simulation.

Preface

This thesis is written for the tolerance analysis in a 3-dimensional situation based on the KavoKerr' s dental X-ray device. I want to thank KavoKerr for providing the device, investing time and money in 3D scanning as well as tolerance analysis development.

I want to thank all the people from Cascade involved in the 3D scanning. It helped me to learn a lot in the 3D scanning field. I am grateful to Mika Katainen and Esa Mäkeläinen for providing useful information in tolerance analysis that helped me to reach the thesis goals. Thanks to all people in the KavoKerr Mechanical Engineering team for being nice and giving help when I needed it. I also owe much to Professor Kevin Otto, who has supported me throughout my thesis and volunteered for supervising this thesis. Lastly, I want to thank my advisor Rurik Englund. Your ability to listen, motivate and keep pushing me when needed was beyond description.

Espoo, November 30, 2018

Xi Fan

Table of contents

Abstract
Preface
Table of contents 5

Acronyms 7

1 Introduction 8

1.1 KavoKerr 8

1.2 The research problem 9

1.3 Goals for the Research 9

1.4 Research methods 9

1.5 Related Research 10

2 Tolerance analysis 11

2.1 Tolerance stack-up analysis process 12

2.2 3D Tolerance Calculation 19

2.3 Monte Carlo Simulation 26

3 3D scanning 29

3.1 3D scanning Technique 30

3.2 3D optical scanner 31

3.3 3D Laser Scanner 33

3.4 Strengths and weaknesses 34

4 Analysis 35

4.1 Tolerance stack-up analysis 35

4.2 Analysis of 3D scanning data 39

4.3 Crystal Ball Monte Carlo tolerance analysis 43

5 Solution 49

5.1 X axis error 49

5.2 Y axis error 51

5.3 Z axis error 53

6 Future research 55

7 Summary 57

List of references 60

List of appendices 61

Appendices

Acronyms

ALS	Airborne Laser Scanners
CMM	Coordinate Measuring Machine
DFR	Datum Reference Frames
DLM	Direct Linear Method
HTM	Homogeneous Transformation Matrix
LSL	Lower Specification Limits
RSS	Root Sum Square
RMS	Root Mean Square
T-Map	Tolerance-Map
TLS	Terrestrial Laser Scanning
USL	Upper Specification Limits

1 Introduction

Tolerance has a critical connection between engineering design and manufacturing industry as can be seen in Figure 1. Tolerance control can ensure product quality and productivity. Without tolerance control, the poorly performing product will be soon out of the market. Engineering designers always want to have a tight tolerance because it can ensure part's fit and the final functionality of a product. On the contrary, manufacturing industries want to have a loose tolerance because it means less expensive and easier to manufacture parts. It is essential to find a tolerance value to balance between engineering design and manufacturing.

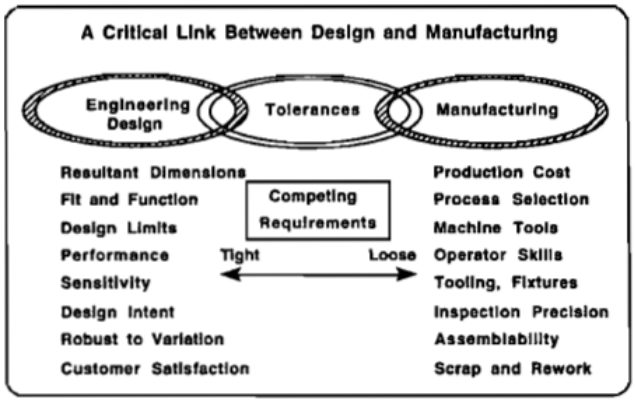

Figure 1 The effects of assigned tolerance are far-reaching. (Gao, Chase and Magleby, 1998)

3D scanning is a recently developed technology. The first 3D scanning system based on imaging triangulation were installed for industrial applications at the end of the eighties. It is mainly used for surface inspection, deformation analysis and comparative measurements. (Bernd, 2014) Nowadays in the industrial fields, 3D scanning technology is widely used for product inspection as well as reverse engineering in manufacturing and designing area. Its basic principle is to capture data from objects in the real world and bring them into the digital pipeline. (Laing, 1994) With the help of 3D scanning technology tolerances can be controlled more easily.

1.1 *KavoKerr*

KavoKerr combines two global companies called Kavo and Kerr to provide dental excellence and service as a single partner for the dental community. Kavo has been focusing on innovation and quality in dental products and services for more than 100 years. Kerr has

been serving the needs of dental care for over 125 years. KavoKerr in Finland is called Kavo Kerr Group Finland. It is located in Tuusula and has around 400 employees.

1.2 *The research problem*

Tolerances always exist in the physical world and can be easy to ignore, but in the end are critical for product functionality. Product quality depends on measuring manufactured part dimensions for conformance with a defined tolerance. At KavoKerr, most parts are supplied by a variety of suppliers but there exists no good way to inspect incoming product quality. 3D scanning is a promising approach to securing product quality. Besides use in product quality assessment, it can be used in engineering design. A key is issue however is determining the suitability of 3D scanning in these particular tasks and constraints.

A single assembly device contains many parts with each part having many dimensions that need to be manufactured within tolerance. It can be difficult to determine which dimension is crucial for the final assembly from the large number of dimensions. Tolerance analysis is the best way to solve this problem. Separation in 1D, 2D or 3D to complete tolerance analysis is the usual way. The difficulty level increases with increase in dimensions. In this research, a 3D tolerance analysis approach was adopted. There were two research areas that the project sought to answer during the tolerance analysis:

- How to do the tolerance analysis in the 3D case?
- What is the correlation between the real assembly results measured by 3D scanning and Computer-Aided tolerance analysis results?

1.3 *Goals for the Research*

As a practical implication, this research supports the development of individual parts and assembly quality within companies by determining the tolerance variation. Further, this research gives a useful guide for 3D tolerance analysis and advice for using 3D scanning in the future for product inspection and engineering design.

1.4 *Research methods*

Literature review based on Aalto e-library search results and several books recommended by professor and company colleagues formed the theoretical basis for this research. The particular assembly area of the Dental X-ray device used in this research is shown in Figure 2

marked in red. The experiment data were collected from 3D scanning measurements and defined tolerances in drawing. 3D scanning measured five series of parts and then scanned the assembled devices built from those parts. Based on the HTM calculator in Excel, the tolerance analysis results were collected by running Monte Carlo simulations in the Crystal Ball software.

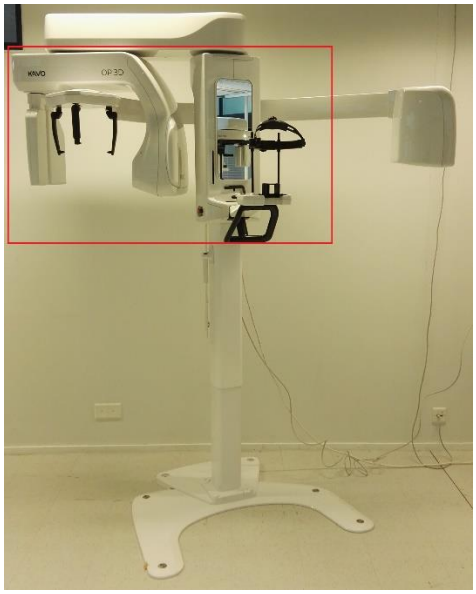

Figure 2 Dental X-ray device.

1.5 *Related Research*

Much research has been done in the design and manufacturing fields relating particularly on tolerance analysis. These include methods for tolerance stack-up analysis based on 1D, 2D or 3D tolerance zones and comparing T-Map, matrix model, unified Jacobian-Torsor model and DLM 3D tolerance analysis methods. The method utilized in this thesis project is Paul Drake's tolerance stack-up process and Daniel Whitney's HTM model for the assembly phase works in an assembly device tolerance analysis.

3D scanning also has a large amount of pre-existing literature, such as 3D scanning device comparisons, improving 3D scanning technology for different applications, and testing 3D scanning method for different applications. This thesis project has the same research area as Teodor Tóth's 3D optical and laser scanner comparison research. However, the comparison purpose in this project differs substantially from prior research with a much more practical point of view.

2 Tolerance analysis

As per Figure 3, tolerance analysis can be separated into tolerance representation and propagation. It also can be represented by five different categories which are device, level, phase, dimensionality and objective. In the future, with the development of mechanical design and manufacturing, the tolerance analysis classification will be more and more complicated. (Chen *et al.*, 2014)

Tolerance analysis can be done using manual or CAT software, such as VisVSA, 3DCS, Crystal Ball and CETOL. There are two levels in tolerance analysis: part and assembly. Based on different assembly methods, sequences and components, the stack up effect of the assembly can be described either in explicit or implicit function. Tolerance analysis can be used for design, process planning, manufacturing and inspection. The objectives for using tolerance analysis in each sector may be different. When in the design phase, conventional and geometric tolerance ensure that the product meets the functional requirements. The Cp, Cpk and variation transfer will decide the product manufacturing process and complexity. In the inspection phase, tolerance analysis will be conducted by data process and quality estimate. According to dimensionality, there are 1D, 2D and 3D tolerance analyses. A different method such as worst case, statistical or Monte Carlo simulation is used to do the different dimensional analyses. Objectives of tolerance analysis can be divided into rigid or flexible assembly. Rigid assembly is surface-based and needs only shape closure. Flexible assembly is point-based and needs shape and force closure at the same time. (Chen *et al.*, 2014)

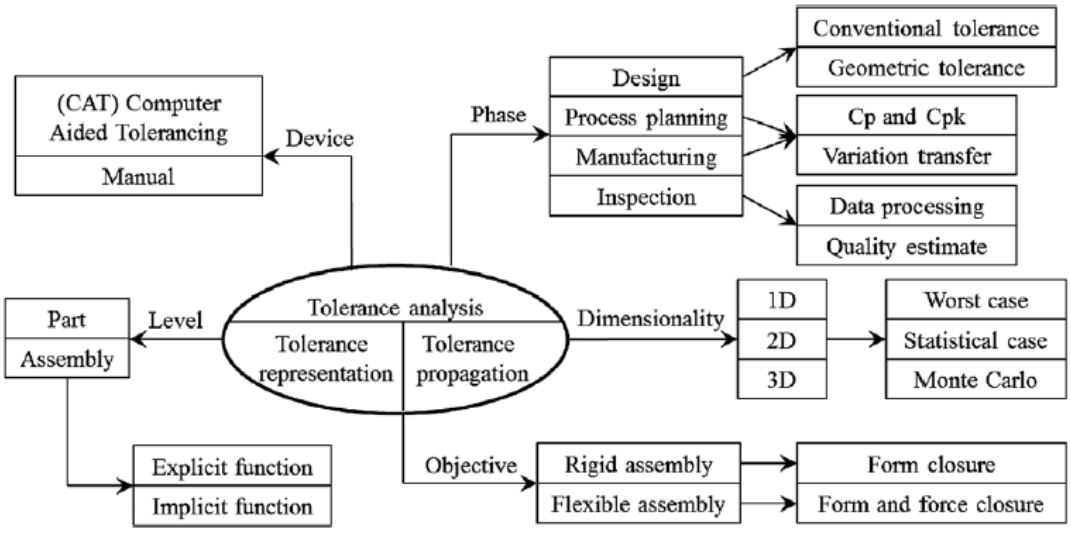

Figure 3 Categories of tolerance analysis. (Chen *et al.*, 2014)

2.1 *Tolerance stack-up analysis process*

Figure 4 shows the traditional process for tolerance stack-up analysis. (Drake, 1999)

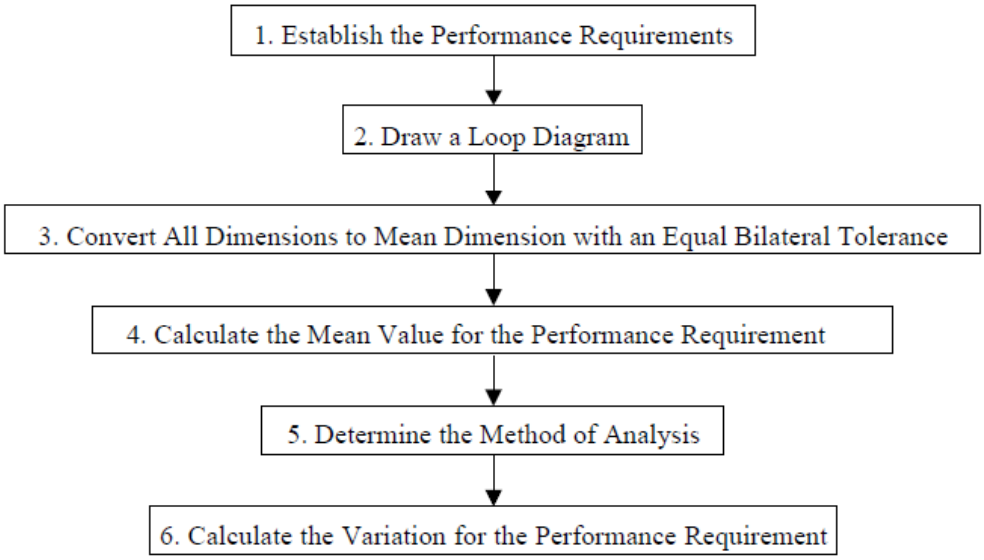

Figure 4 Tolerance analysis process (Drake, 1999)

2.1.1 Establish the performance Requirements

The first step is to identify the requirements for the assembly system. These requirements usually are the critical criteria that need to be analyzed. They also ensure the functionality of the product. (Drake, 1999) For example, the requirement in Figure 5 is the minimum gap that needs to be smaller than a certain value.

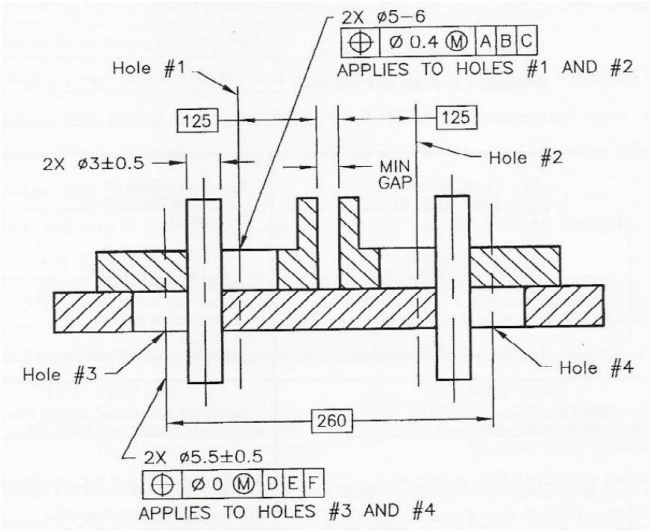

Figure 5 tolerance stack-up analysis example (*Tolerance Stack-Up Analysis*, no date)

2.1.2 Draw a loop diagram

Loop diagrams can be divided to 1D, 2D and 3D tolerance zones as shown in Figure 6. (Lin and Zhang, 2001) Figures 7, 8 and 9 show examples of 1D, 2D and 3D loop diagrams. Compared to a 1D loop diagram, a 2D and 3D tolerance loop diagram becomes much more complicated. The first part with the starting point automatically has the local coordinate system called DFR. DFR is used to locate the feature in each part. Every part has its own DFR during the transformation. When creating a loop diagram either in 1D, 2D or 3D, there are some rules that need to be obeyed, as Drake (Drake, 1999, p. 433) states:

i. Loops must pass through every part and every joint in the assembly
ii. A single vector loop may not pass through the same part or the same joint twice, but it may start and end in the same part.
iii. If a vector loop includes the same dimension twice, in opposite directions, the dimension is redundant and must be omitted.
iv. There must be enough loops to solve for all the kinematic variables (joint degrees of freedom).

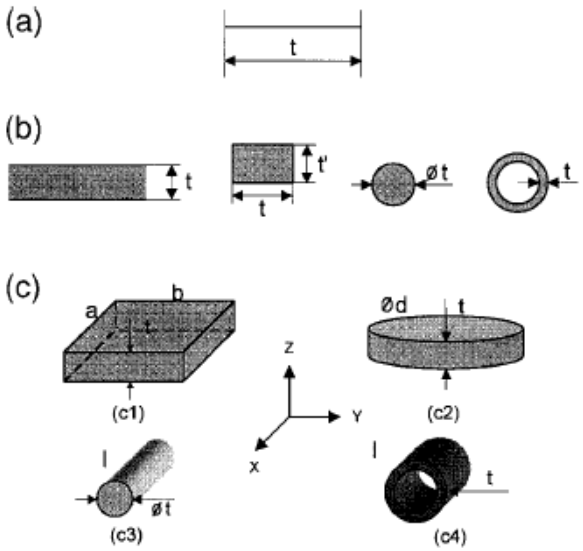

Figure 6 Typical tolerance zone (a) 1D, (b) 2D, (c) 3D (Lin and Zhang, 2001)

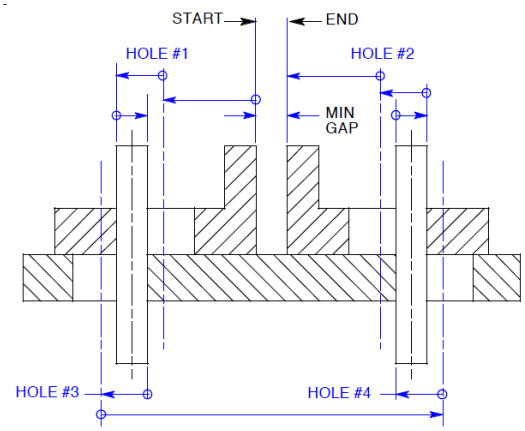

Figure 7 1D Loop diagram. (*Tolerance Stack-Up Analysis*, no date)

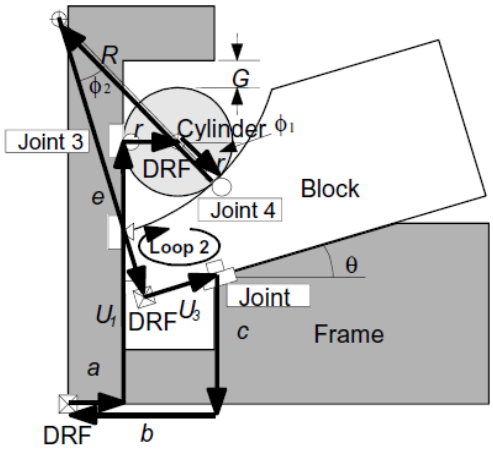

Figure 8 2D loop diagram. (Chase, 1999).

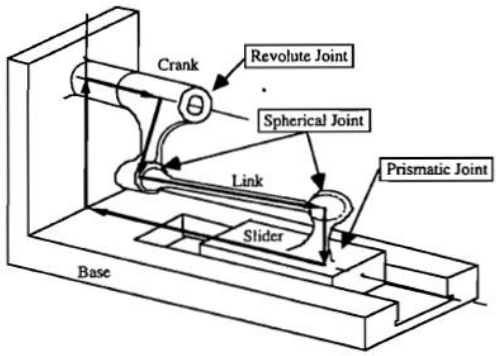

Figure 9 3D loop diagram. (Gao, Chase and Magleby, 1998)

2.1.3 Convert all the dimensions

After drawing a complete loop diagram, the next step is to find out all the dimensions in the loop diagram and convert all the dimensions to equal bilateral tolerance. It is easier to do

tolerance analysis when converting unilateral tolerances to equal bilateral tolerances. Sometimes in the drawing, unilateral tolerances may be marked specifically because of manufacturing issues. Figure 10 shows the different dimension with unilateral tolerances. Those dimensions all have the same meaning. (Drake, 1999)

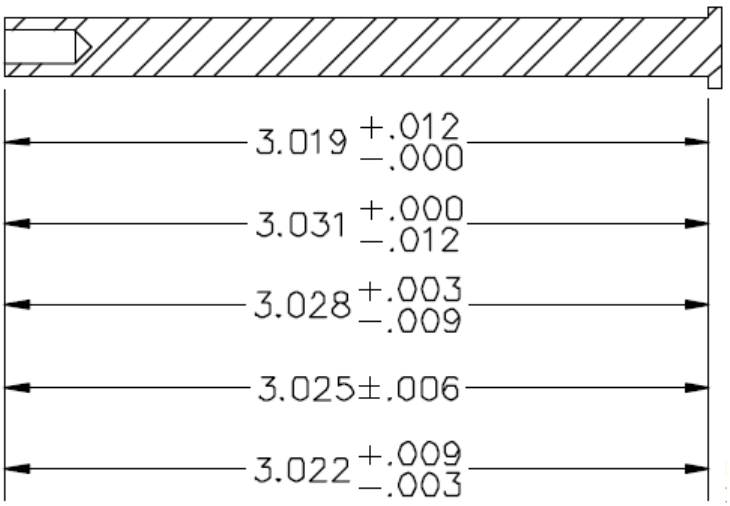

Figure 10 methods to dimension the length of a shaft. (Drake, 1999)

There are four steps in converting unilateral tolerance to an equal bilateral tolerance. (Drake, 1999)

i. Adding up the dimension and tolerances to get an upper and lower limit. (For example, 3.022 + 0.009/-0.003 = 3.031 upper limit / 3.019 lower limit)
ii. Using the upper limit subtract lower limit to get a total tolerance band. (3.031-3.019=0.012)
iii. Dividing the tolerance band by two to get an equal bilateral tolerance. (0.012/2 =0.006)
iv. Using upper limit subtract the equal bilateral tolerance (3.031-0.006=3.025) or using lower limit add the equal bilateral tolerance (3.019+0.006=3.025) to get the mean dimension.

2.1.4 Mean Value of the requirements

The mean value of the requirements can be defined through the loop diagram locations. Before starting to calculate the mean value of the requirements, there are several things that

need to be defined such as the direction of the vector. Figure 11 shows an example of 3D vector direction. The vector direction can be decided freely.

The mean value of the gap in 1D loop diagram shown in Figure 7 is the sum of the total positive and negative vector of mean dimensions shown in Table 1. In 2D loop diagram shown in Figure 12, the mean value of the gap can be calculated with Equation 1. In the 3D loop diagram, the mean value of requirements needs to use HTM to calculate the results.

$$\text{Gap} = U_1 \sin(-90) + r \sin(180) + r \sin(-90) + g \sin(0) + f \sin(90) \quad (1)$$

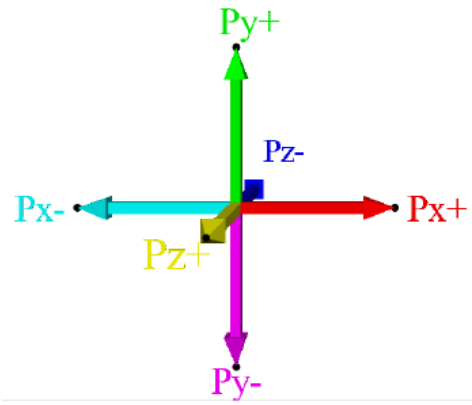

Figure 11 Example of the 3D vector direction. (Botero, Hernández and Fernández, 2014)

Table 1 Data of all the dimensions from the figure 6 for calculating mean value of the requirement. (*Tolerance Stack-Up Analysis*, no date)

VECTOR DIMENSIONS		TOLERANCES	
–	+	±	PART
125		0.0	Basic Dim.
3		0.7	Hole #1/2
	3	0.5	Pin
3		0.5	Hole #3/2
	260	0.0	Basic Dim.
3		0.5	Hole #4/2
	3	0.5	Pin
3		0.7	Hole #2/2
125		0.0	Basic Dim.
– 262	+ 266	± 3.4	TOTALS

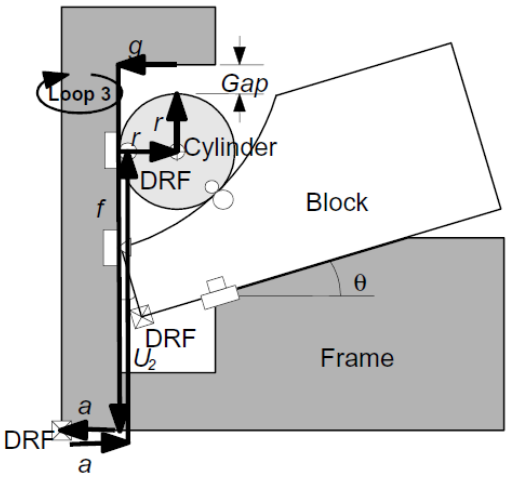

Figure 12 Open loop for calculating the 2D mean value of the requirement. (Chase, 1999)

2.1.5 Methods of tolerance analysis

Figure 13 shows the three methods of doing tolerance analysis, namely worst-case analysis, statistical analysis and sampled analysis. (Arras and Merode, 2012)

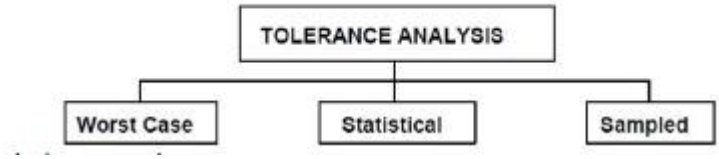

Figure 13 Tolerance analysis methods. (Arras and Merode, 2012)

Among these three methods, the worst-case analysis is the easiest way to calculate tolerance maximum and minimum values. It will only provide the information about if the stack-up tolerance results over the specified tolerance limits or not. Figure 14 shows the basic rule to calculate tolerance using the worst-case method. In this method, every tolerance value is assumed to be equal to one of the tolerance limits. After all the tolerance limits are added together, the extreme stack-up condition can be shown in the results. The worst-case tolerance analysis guarantees 100% of the product functionality when parts are assembled without considering the variation of the tolerance between the parts. The biggest disadvantage of this method is that the tolerance value in every component is very tight. Tight tolerance can

cause a high cost to manufacture the product and inspect product quality. (Arras and Merode, 2012)

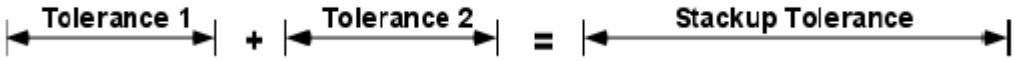

Figure 14 Worst case model. (Arras and Merode, 2012)

Statistical variation analysis model is based on statistical principles. This method can loosen the component's tolerances without influencing the quality standard. Figure 15 shows the basic principle behind statistical variation analysis. The dimension's value is taken randomly within the tolerance limit. Every part dimension's variation can be modeled as a statistical distribution. Adding these parts distributions together makes it possible to predict the assembly measurement distribution. Compared to worst-case tolerance analysis, a statistical analysis gives better flexibility in design and closer to standard tolerance setting. (Arras and Merode, 2012)

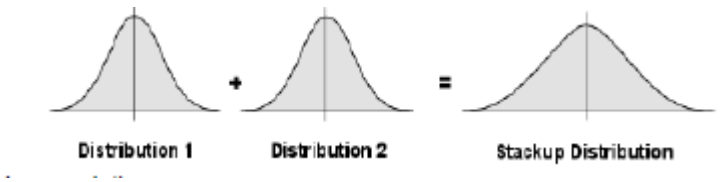

Figure 15 Statistical variation analysis model. (Arras and Merode, 2012)

2.1.6 Performance requirements variation

The next step is calculating the variation for the performance requirements. There are three main causes of variation in the assembly. The first one is individual part dimensional variation. The second one is the variation of geometric features. The last one is small kinematic adjustments variation. (Gao, Chase and Magleby, 1998)

When using the worst-case model for analysis of the gap variation, the result is equal to the sum of the individual tolerances. In table 1, the variation of the gap is ±3.4. Based on the same tolerance value shown in table 1 and using the RSS model to calculate the variation of the gap the final results are (Drake, 1999):

$$t_{rss} = \sqrt{[0^2+0.7^2 + 0.5^2 + 0.5^2 + 0^2 + 0.5^2 + 0.5^2 + 0.7^{2+}0^2} = 1.4 \quad (2)$$

2.2 3D Tolerance Calculation

The HTM has been widely used in the projective geometry and robotics fields. It also can be used in assembly to locate the parts and locate the feature on parts. In the HTM model, every part and every feature on parts has a base coordinate frame. The base coordinate frame can be changed based on the parts and features transformation route. Every HTM represents the parts or the features on parts relative position to the last parts or last feature on parts. In 3D space, HTM contains three rotational degrees and three translational positions. (Whitney, 2004)

2.2.1 HTM of Nominal Location

This matrix shows the points or vectors relative position for one coordinate frame to another coordinate frame. It is important to know that the whole coordinate frame will be represented by the matrix, not just a single point. Figure 16 illustrates that the transform T contains a translational part p and a rotational part R. The transform mathematical form can be seen in Equation 3. (Whitney, 2004)

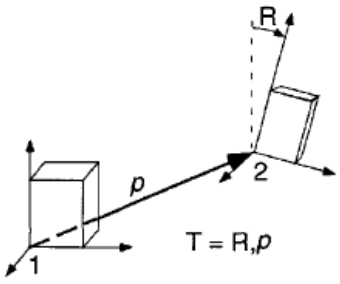

Figure 16 Schematic Representation of a transform. (Whitney, 2004)

$$T = \begin{bmatrix} R & p \\ 0^T & 1 \end{bmatrix} \tag{3}$$

Translation part p is a 3×1 displacement vector. It shows the new coordination frame position relative to the old one. Rotational part R is a 3×3 rotating matrix. It means the orientation of the new frame relative to the old one. The transformation T can be expressed as Equation 4. (Whitney, 2004)

$$T = \begin{bmatrix} r_{11} & r_{12} & r_{13} & p_1 \\ r_{21} & r_{22} & r_{23} & p_2 \\ r_{31} & r_{32} & r_{33} & p_3 \\ 0 & 0 & 0 & 1 \end{bmatrix} \quad (4)$$

Transform T can be used to calculate the point relative position compared to the first coordinate system. The coordinate point is given by the following equation. (Whitney, 2004)

$$p = \begin{bmatrix} x \\ y \\ z \end{bmatrix} \quad (5)$$

The equations 6, 7 and 8 represent how matrix R can be calculated by rotating each coordinate axis once. The equation 9 means the new coordinate system w can be obtained from rotating the original coordinate system u in y axis 90° first and then in the new z axis position rotate 90°. (Whitney, 2004)

$$rot\ (x, \theta) = \begin{bmatrix} 1 & 0 & 0 & 0 \\ 0 & \cos\theta & -\sin\theta & 0 \\ 0 & \sin\theta & \cos\theta & 0 \\ 0 & 0 & 0 & 1 \end{bmatrix} \quad (6)$$

$$rot\ (y, \beta) = \begin{bmatrix} \cos\beta & 0 & \sin\beta & 0 \\ 0 & 1 & 0 & 0 \\ -\sin\beta & 0 & \cos\beta & 0 \\ 0 & 0 & 0 & 1 \end{bmatrix} \quad (7)$$

$$rot\ (z, \alpha) = \begin{bmatrix} \cos\alpha & -\sin\alpha & 0 & 0 \\ \sin\alpha & \cos\alpha & 0 & 0 \\ 0 & 0 & 1 & 0 \\ 0 & 0 & 0 & 1 \end{bmatrix} \quad (8)$$

$$w = rot(y, 90) rot(z, 90) u \quad (9)$$

Transform without reorientation as just a simple reposition of a frame can be shown as below: (Whitney, 2004)

$$T_{tras} = \begin{bmatrix} 1 & 0 & 0 & p_x \\ 0 & 1 & 0 & p_y \\ 0 & 0 & 1 & p_z \\ 0 & 0 & 0 & 1 \end{bmatrix} = trans(p_x, p_y, p_z) \quad (10)$$

T and R multiplied with each other will get a different result when the sequence changes even though they have the same meaning. For example, in equations 11 and 12, T and R

multiply with each other with a different sequence, but in Figure 17, they all end up at the same position of new coordination system. (Whitney, 2004)

$$rot(z,90)trans(p_x,0,0) \tag{11}$$

$$trans(p_x,0,0)rot(z,90) \tag{12}$$

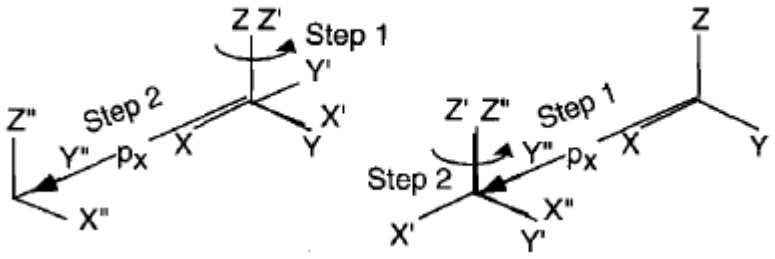

Figure 17 Illustration of two ways of interpreting equation. (Whitney, 2004)

Calculated results based on Equation 11 are shown below: (Whitney, 2004)

$$rot\ (z,90)trans(p_x,0,0) = \begin{bmatrix} 0 & -1 & 0 & 0 \\ 1 & 0 & 0 & p_x \\ 0 & 0 & 1 & 0 \\ 0 & 0 & 0 & 1 \end{bmatrix} \tag{13}$$

Calculated results based on Equation 12 are shown below**:** (Whitney, 2004)

$$trans(p_x,0,0)rot\ (z,90) = \begin{bmatrix} 0 & -1 & 0 & p_x \\ 1 & 0 & 0 & 0 \\ 0 & 0 & 1 & 0 \\ 0 & 0 & 0 & 1 \end{bmatrix} \tag{14}$$

According to the different calculation results, defining the sequence of coordinate system translations and rotations is really important. (Whitney, 2004)

2.2.2 HTM of Variation transforms

During a transformation, there can be some small changes in the transformation. These small changes are the error of the transformation. The error during the transform is either in rotation R or translation p. When in variation analysis, it is convenient to use the same mathematics frame to define both the nominal and varied location of a part or a feature on a part. The error equation in R and p are shown below. (Whitney, 2004)

$$Drot\ (x, \delta\theta_x) = \begin{bmatrix} 1 & 0 & 0 & 0 \\ 0 & \cos\delta\theta_x & -\sin\delta\theta_x & 0 \\ 0 & \sin\delta\theta_x & \cos\theta\delta\theta_x & 0 \\ 0 & 0 & 0 & 1 \end{bmatrix} \quad (15)$$

$$Drot\ (y, \delta\theta_y) = \begin{bmatrix} \cos\delta\theta_y & 0 & \sin\delta\theta_y & 0 \\ 0 & 1 & 0 & 0 \\ -\sin\delta\theta_y & 0 & \cos\delta\theta_y & 0 \\ 0 & 0 & 0 & 1 \end{bmatrix} \quad (16)$$

$$Drot\ (z, \delta\theta_z) = \begin{bmatrix} \cos\delta\theta_z & -\sin\delta\theta_z & 0 & 0 \\ \sin\delta\theta_z & \cos\delta\theta_z & 0 & 0 \\ 0 & 0 & 1 & 0 \\ 0 & 0 & 0 & 1 \end{bmatrix} \quad (17)$$

$$Dtrans(d_x, d_y, d_z) = \begin{bmatrix} 1 & 0 & 0 & d_x \\ 0 & 1 & 0 & d_y \\ 0 & 0 & 1 & d_z \\ 0 & 0 & 0 & 1 \end{bmatrix} \quad (18)$$

Equation 19 shows how the errors transform DT can be created by multiplying these equations together. (Whitney, 2004)

$$DT = \begin{bmatrix} 1 & -\delta\theta_z & \delta\theta_y & d_x \\ \delta\theta_z & 1 & -\delta\theta_x & d_y \\ -\delta\theta_y & \delta\theta_x & 1 & d_z \\ 0 & 0 & 0 & 1 \end{bmatrix} \quad (19)$$

If DT is an error during the T transformation, then T’ can be calculated as DT·T as in Figure 18. (Whitney, 2004)

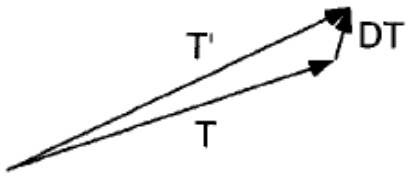

Figure 18 Properties of the error transform.

2.2.3 HTM for an Assembly

The left side of Figure 19 shows the ideal situation during assembly and the right side the real assembly situation with some introduced errors. In this case, the error part is a feature

F_{2B} on part B. This can influence the relationship between feature F_{2B} and F_{1C} as well as the final location of C. (Whitney, 2004)

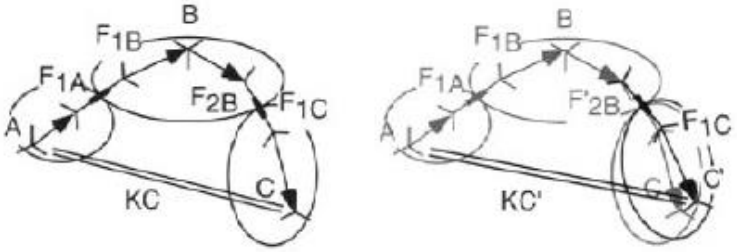

Figure 19 Parts joined by a chain of frames to deliver a KC. (Whitney, 2004)

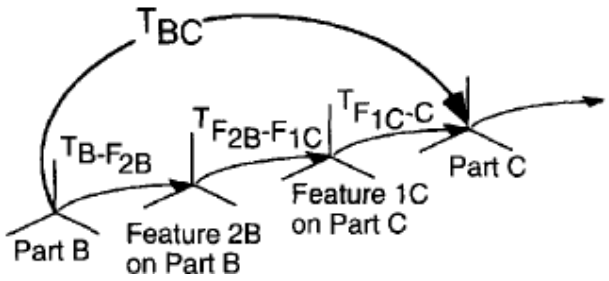

Figure 20 Illustration the features contained from part B to C. (Whitney, 2004)

In the nominal situation, Figure 20 describes how the frame transforms from part B to C in detail. The transform equation from A to C can be shown : (Whitney, 2004)

$$T_{AC} = T_{AB}T_{BC} \tag{20}$$

$$T_{AB} = T_{A-F_{1A}}T_{F_{1A}-F_{1B}}T_{F_{1B}-B} \tag{21}$$

$$T_{BC} = T_{B-F_{2B}}T_{F_{2B}-F_{1C}}T_{F_{1C}-C} \tag{22}$$

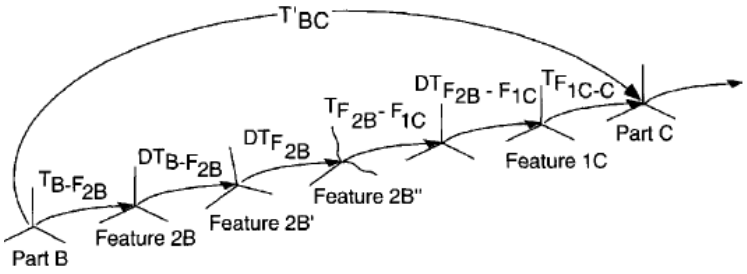

Figure 21 Illustrating the errors from part B to C. (Whitney, 2004)

Figure 21 shows the frame of error when transforming part B to part C. $DT_{B-F_{2B}}$ is the misplacement including location and orientation. DF_{2B} is the feature F_{2B} shape error. $DT_{F_{2B}-F_{1C}}$ is the feature relationship error between part B and C. The final equation for transforming part B to C including all errors is shown in Equation 23: (Whitney, 2004)

$$T'_{BC} = T_{B-F_{2B}} T_{F_{2B}-F_{1C}} T_{F_{1C}-C} (DT_{B-F_{2B}} + DF_{2B} + DT_{F_{2B}-F_{1C}}) \tag{23}$$

The transform equation of varied KC' is shown below: (Whitney, 2004)

$$T'_{AC} = T_{AB} T'_{BC} \tag{24}$$

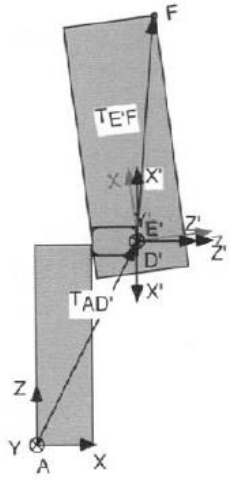

Figure 22 Example of assembly calculation. (Whitney, 2004)

Figure 22 shows the example of assembly calculation. Without any error from point A to point F based on the coordinate system in part A, T_{AF} can be calculated as Equation 25. Transform T'_{AF} includes all the errors such as the misallocated peg and misoriented hole

from Point A to point F. The equation to calculate T'_{AF} can be written as in Equation 26. (Whitney, 2004)

$$T_{AF} = T_{AD}T_{DE}T_{EF} \tag{25}$$

$$T'_{AF} = T_{AD'}T_{D'E'}T_{E'F} \tag{26}$$

$$T_{DE} = T_{D'E'} = rot\ (Z, 180) \tag{27}$$

There are two methods to solve the frame or feature displacement problems to get $T_{AD'}$. One way is to use the original coordinate system and another is to use a new coordinate system instead of the original one. In Figure 23 on the left side A coordinate system is used to define D position: (Whitney, 2004)

$$DT_{AD} = trans(0,0,DZ) \tag{28}$$

$$T_{AD'} = T_{AD}DT_{AD} \tag{29}$$

On the right side D coordinate system is used for calculation: (Whitney, 2004)

$$DT_{AD} = trans(-DX,0,0) \tag{30}$$

$$T_{AD'} = T_{AD}DT_{AD} = T_{AD}T_{DD'} \tag{31}$$

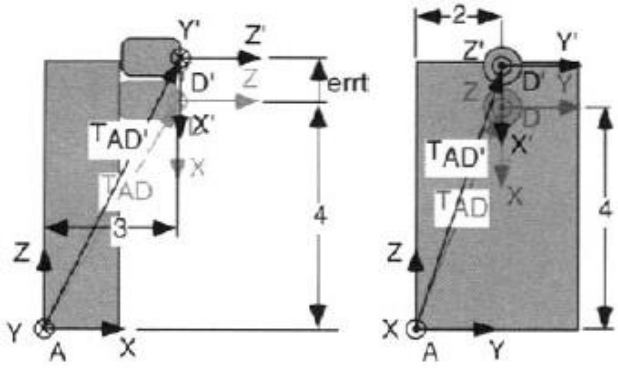

Figure 23 Illustrate how to calculate the varied transform without rotation. (Whitney, 2004)

Figure 24 shows the misallocated hole in y axis. $T_{E'F}$ can be calculated as follow: (Whitney, 2004)

$$T_{E'F} = T_{E'E}T_{EF} \tag{32}$$

$$T_{E'E} = rot\ (y, erra) \tag{33}$$

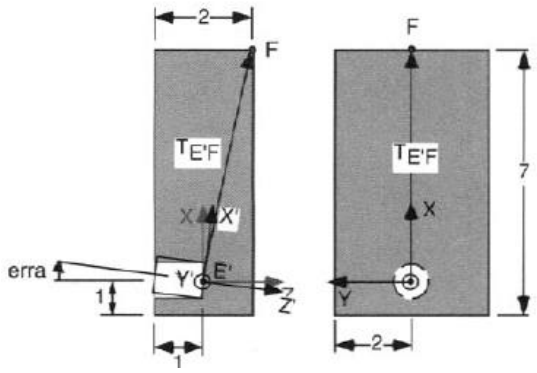

Figure 24 Illustrate how to calculate misoriented hole. (Whitney, 2004)

2.3 *Monte Carlo Simulation*

Monte Carlo simulation can be used for predicting the variation. It is a relatively easy method for nonlinear statistical tolerance analysis. The process for Monte Carlo simulation can be described as follows (Bryan Dodson, Patrick Hammett, Rene Klerx, 2014) :

i. Define the simulation system.
ii. Decide the system input variation behavior.
iii. Generates a random value from input variation.
iv. Compute the output in the system.
v. Repeat step 3 and 4 until the results are steady.

2.3.1 Determining inputs variation

The variation of inputs can be determined in three ways. The first one is assuming a distribution and a process capability index C_{pk} equivalent to ±4 standard deviation which is 1,33 based on the general tolerance standards. The second method is requesting the actual realized statistical data from your company or the supplier. When requesting the data, there is a need to ensure that the timeframe for sample collection was sufficiently long and includes all the possible variation sources such as tooling changes, equipment changes and raw material differences. The third way is collecting your own statistical data. When you are collecting your own data, the most important thing is to make sure that as many variation sources are included as possible. (Bryan Dodson, Patrick Hammett, Rene Klerx, 2014)

2.3.2 Random number generators

The core of any simulation is the random number generation. Transforming random numbers from unit uniform distribution can be used to generate random numbers from specific distributions. Figure 25 shows the unit uniform distribution. It is uniformly distributed from zero to one. (Bryan Dodson, Patrick Hammett, Rene Klerx, 2014)

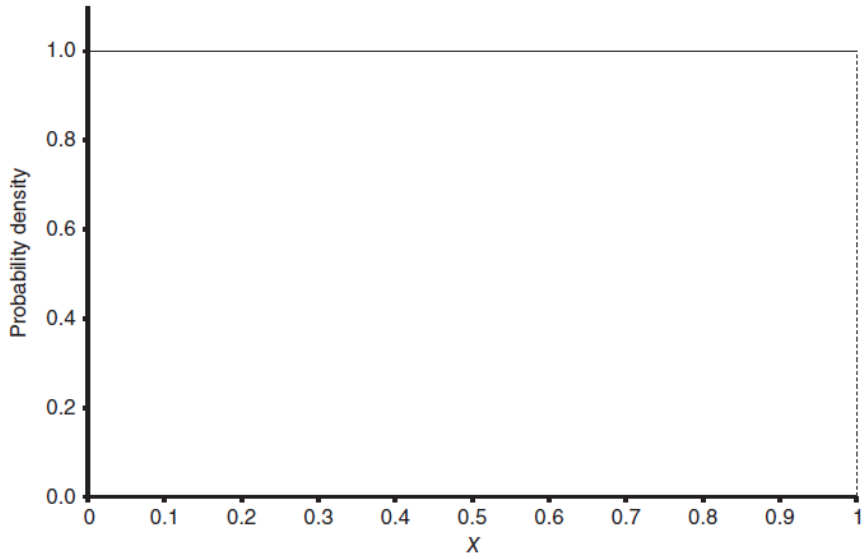

Figure 25 Unit uniform probability density function. (Bryan Dodson, Patrick Hammett, Rene Klerx, 2014)

Nearly all programming languages and even simple electronic spreadsheets have a uniform random number generator. Using the algorithms to generate the random numbers is extremely efficient and suits most practical purposes. Figure 26 shows other methods used to generate random numbers. (Bryan Dodson, Patrick Hammett, Rene Klerx, 2014)

Distribution	Probability Density Function	Random Number Generator
Uniform	$f(x) = \frac{1}{b-a}, \quad a \le x \le b$	$x = a + (b-a)r$
Exponential	$f(x) = \lambda e^{-\lambda x}, \quad 0 < x < \infty$	$x = -(1/\lambda) \ln r$
Normal	$f(x) = \frac{1}{\sigma\sqrt{2\pi}} \exp\left[-\frac{1}{2}\left(\frac{x-\mu}{\sigma}\right)^2\right], \quad -\infty < x < \infty$	$x_1 = \left[\sqrt{-2 \ln r_1} \cos(2\pi r_2)\right] \sigma + \mu$
Lognormal	$f(x) = \frac{1}{\sigma x\sqrt{2\pi}} \exp\left[-\frac{1}{2}\left(\frac{\ln x - \mu}{\sigma}\right)^2\right], \quad x > 0$	$x_1 = \exp\left[\sqrt{-2 \ln r_1} \cos(2\pi r_2)\right] \sigma + \mu$
Weibull	$f(x) = \frac{\beta x^{\beta-1}}{\theta^\beta} \exp\left(-\frac{x}{\theta}\right)^\beta, \quad x > 0$	$x = \theta(-\ln r)^{1/\beta}$

Figure 26 Random number generators. (Bryan Dodson, Patrick Hammett, Rene Klerx, 2014)

2.3.3 Validation

It is important to validate the model when it complete. The common validation process is (Bryan Dodson, Patrick Hammett, Rene Klerx, 2014) :

i. Compare the mean theoretical value and standard deviation of inputs value.
ii. Compare histogram shape constructed by each input to the expected distribution shape.
iii. Randomly select several rows from the simulation and check the output are correct or not.

Enough repetitions can bring steady-state results. One thousand repetitions are acceptable when calculating means and variation. At least one million iterations can get the most reasonable results when designing a product that needs to meet a specification with a failure rate of less than 20 parts per million. (Bryan Dodson, Patrick Hammett, Rene Klerx, 2014)

3 3D scanning

Nowadays, more and more industries use 3D scanning devices to ensure product quality. These quality assurance devices are simple to operate and get an accurate measuring data compare to traditional measurement. 3D scanning perfectly combines the reverse engineering and inspection two purposes together shown in Figure 28. A 3D scanner can be used to get the geometry data out of the physical product. It can also be used to build a virtual 3D model from the scanned project. (Brajlih *et al.*, 2011) Figure 28 shows the 3D scanning digitizing process for inspection and reverse engineering. (Kuş, 2009)

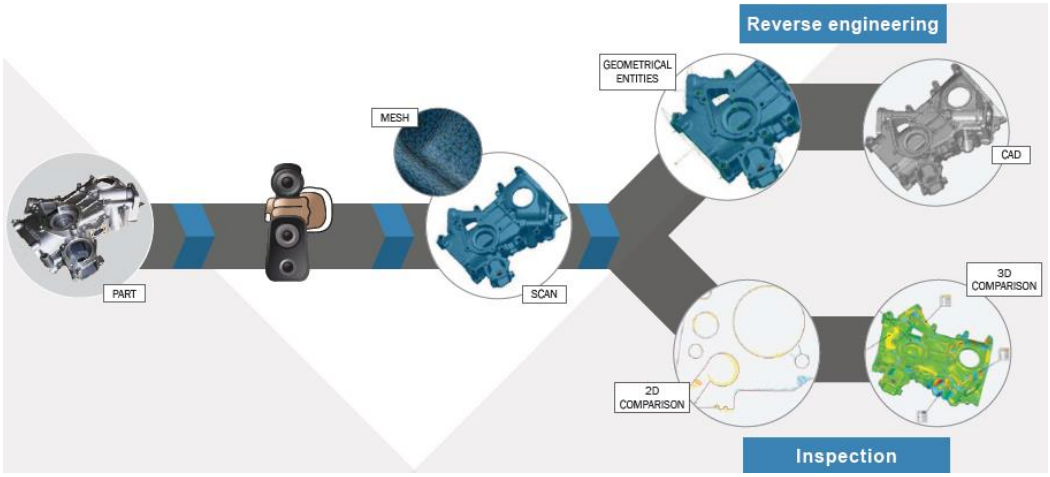

Figure 27 Scanning two main purpose. (Laing, 1994)

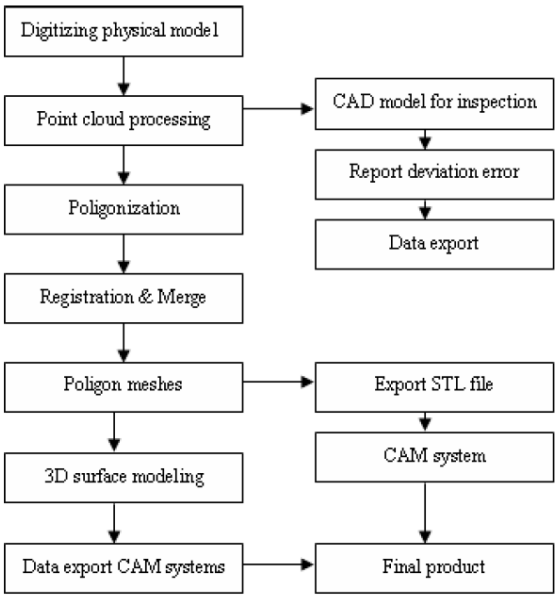

Figure 28 3D digitizing process. (Kuş, 2009)

When the 3D scanning data are not structured, it usually is of a point cloud or triangle mesh form. After merging data into a complete model, the computer software processes the scanning data correcting errors and improving data quality. The final virtual 3D part looks the same as a physical 3D scanning part. (Laing, 1994)

3.1 *3D scanning Technique*

There exists mainly two methods that can acquire the digital data of the 3D object as shown in Figure 29. These are the tactile and non-tactile method. Tactile methods get data from a 3D contact scanner. It usually uses a probe to contact the object's surface and record position. The probe is usually located at the end of an articulated mechanical arm such as a robotic arm. The recorded position forms a point cloud and generates a 3D mesh. A CMM is a high accuracy 3D contact scanner and is often used in the manufacturing industry. 3D contact scanner scanning process is slow and it is not suitable for scanning delicate objects such as artworks. (Varady, Martin and Cox, 1997)

Non-contact methods can get data from a non-contact scanner. Non-contact 3D scanners have high accurate point clouds as a result. It can be divided into passive or active 3D scanners. The active scanner detects radiation or light reflection generated by the device itself. Examples of this are the 3D laser scanner and 3D optical scanner. Passive scanners rely on detecting ambient radiation reflections and are used in stereoscopic video scanners and photometric scanners. (Abdel-Bary Ebrahim, 2011)

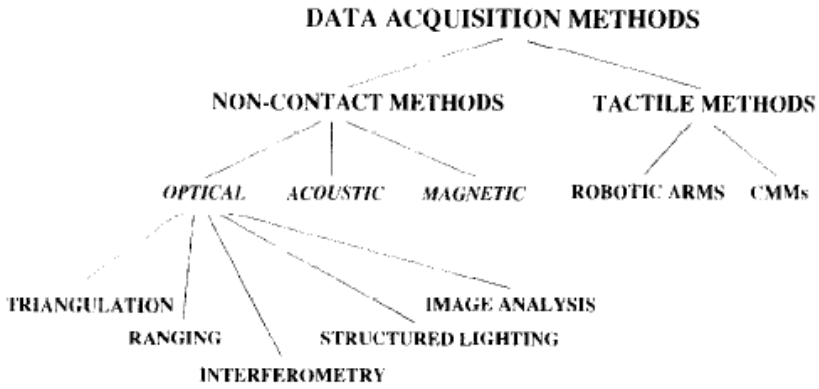

Figure 29 Classification of data acquisition methods. (Varady, Martin and Cox, 1997)

Triangulation principle shown in Figure 30 is one of the 3D non-contact active techniques. It is a method to deduce the object position from the location and angles between light

sources and photo sensing devices. The light source can be a laser or other high energy light source. The distance between the photosensitive camera and a high energy light source is known. The high energy light source project to the surface point with a prespecified angle. The photosensitive camera angle can be determined by the reflection of the surface. Then the surface point location can be calculated from the known angle and distance. The accuracy of results by using the triangulation principle is based on the resolution of the photosensitive device and the distance between the object surface and the scanner. (Varady, Martin and Cox, 1997)

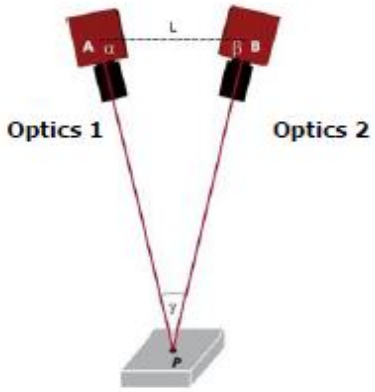

Figure 30 Triangulation principle. (Funke, 2016)

3.2 *3D optical scanner*

Figure 31 shows an example of a 3D optical scanner structure and how it looks like during the scanning. The 3D optical scanner uses the triangulation principle in the scanning system. ATOS Triple Scanner shown in Figure 32 also uses this principle. Based on the stereo camera principle, two cameras record the precise fringe pattern projected to the product surface. The beam path of two cameras and projector are calibrated in advance. According to these three different ray intersections, the 3D surface point can be calculated. These devices use blue light for projection. The blue light can filter other light interference effectively during the scanning. (*ATOS Triple Scan – Industrial Optical 3D Digitizer*, no date)

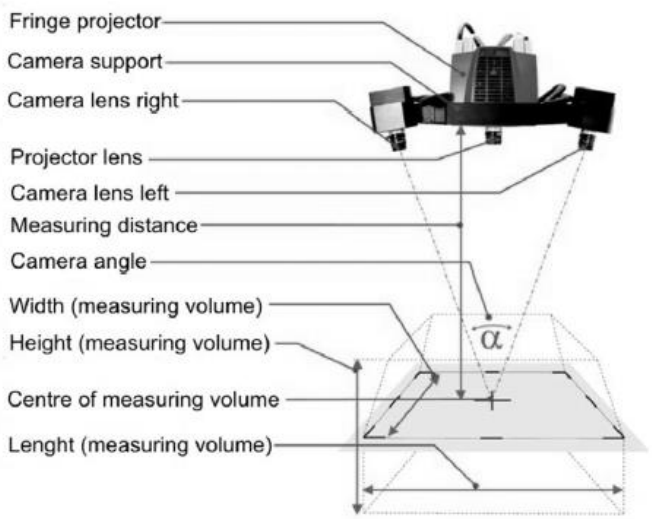

Figure 31 Example of 3D scanner schematics. (Brajlih *et al.*, 2011)

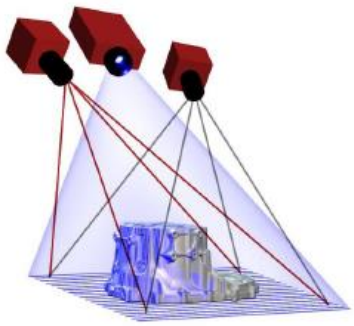

Figure 32 ATOS Triple Scan full-field geometry acquisition. (*ATOS Triple Scan – Industrial Optical 3D Digitizer*, no date)

Scanning from a different angle is required when we want to scan a complete object. 16 million points will be measured in a single scanning. The scanner can either rely on the part geometry to position the data or measuring with the reference points (circular mark stickers) to align 3D data. (Laing, 1994) These positioning methods help the single measurements from different angle transform into a common coordinate system. Those marks can be attached to the scanning objects. (Funke, 2016)

3.2.1 Application for 3D optical scanners

The 3D optical scan can be used in numerous situations. (Brajlih *et al.*, 2011)

- Mechanical engineering:
  Workpiece inspection.

Deformation analysis.

Reverse engineering.

General quality control procedures.

- Civil engineering:
  Building Inspection.
  Customer fit furniture design.
  Cultural heritage protection and renovation.
- Forensics:
  Crime scene investigation.
  Data preservation.
- Textile industry:
  Customer fit product design.
- Movie Industry
  CGI effects creation

3.3 3D Laser Scanner

There are several different types of 3D laser scanners. The ALS, TLS and Hand-held laser scanner are most common 3D laser scanner types. ALS and TLS using the same principle, but the difference is one is air based and another one is ground-based. Hand-held laser scanner using triangulation mechanism to create a 3D virtual product. (Abdel-Bary Ebrahim, 2011)

3.3.1 Application for 3D laser scanners

The 3D laser scanner can be used in lots of different situations such as (Abdel-Bary Ebrahim, 2011)

- Material processing and production
- Construction Industry and civil engineering.
  Create GIS (Geographic information system) maps.
  Site modeling and lay outing
- Entertainment
  Create 3D digital models for both movies and video games.
- Reverse Engineering
- Mechanical applications

- Cultural Heritage

3.4 *Strengths and weaknesses*

Table 2 compares advantages and disadvantages of the 3D scanning and 3D optical scanner. (Engineering & Manufacturing Services, 2017)

Table 2 3D optical and laser scanner strength and weakness.

	3D laser scanner	Structured light (optical) 3D scanner
Advantages	• Able to scan rough surfaces, such as shiny or dark finishes. • Less sensitive to changing light conditions and ambient light. • Portable • Easy to use • Low cost	• Fast scan times • Large scanning area • High resolution • High accuracy • Various price range depends on resolution and accuracy.
Disadvantage	• Errors stack up when scanning volume grows because it uses self-positioning on a more local area. • When positioning targets to minimize errors will increase setup time and limits the area of projects can be scanned efficiently.	• Generate large quantities of data in one scan. • Timing consuming.

4 Analysis

4.1 *Tolerance stack-up analysis*

According to the tolerance stack-up process in Chapter 2. The first step is to define the performance requirements. In this research, the performance requirement is that the position of part 14 center of top surface to the center of part 9 tip shall be within ± 10 mm (Marked with the blue arrow in Figure 33).

The next step as discussed previously is to draw a loop diagram. The 3D loop diagram is shown in Figure 33 below. The part 1 screw hole marked in a red point is the whole loop diagram starting point. DRF is based on this screw hole. Along with the X, Y and Z axes arrows showed in the picture is the positive vector direction. The opposite direction shows the negative sign. The loop goes through 14 parts and 13 joints.

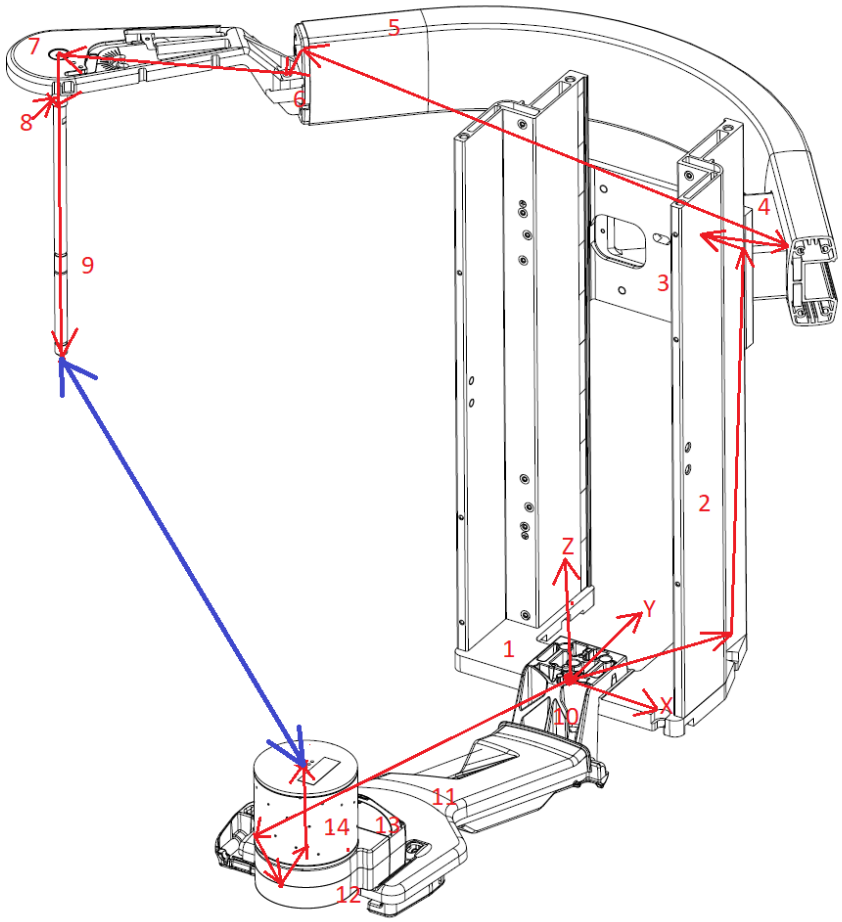

Figure 33 3D loop diagram.

After transferring all the dimension to equal bilateral tolerance, the nominal distance from part 9 pin tip to part 14 top surface center need to be determined. According to the 3D CAD system, Creo dimension measurement, the nominal position in X, Y and Z axes are 649,99mm, 616,52mm and 57,68mm. The 3D HTM calculated nominal distance in three axes should be the same as Creo measurement results. Based on equation 9 and 10. The transformation matrix from Part 1 to part 9 and from part 1 to part 14 can be represented as Table 3 showed below.

Table 3 Parts by parts transformation.

Part 1 to 2	$trans(89, 146{,}2\ , 0)$
Part 2 to 3	$trans(0, 30, 452)$
Part 3 to 4	$trans(-24, 7, 6)rot(z, -51)$ $trans(10{,}155\ , 54{,}11\ , -40)$
Part 4 to 5	$trans(-412{,}03, -407{,}91\ , -40)rot(z, 3)$
Part 5 to 6	$trans(0\ , -20, -27)$
Part 6 to 7	$trans(-12\ , -221\ , 41{,}5)$
Part 7 to 8	$trans(0, 0, -55)$
Part 8 to 9	$trans(0\ , 0, -285)$
Part 1 to 10	$trans(-68, -438, 4{,}06)$
Part 10 to 11	$trans(13, -2{,}1, 25{,}644)$
Part 11 to 12	$trans(55, -105{,}9, 24)$
Part 12 to 13	$trans(0, 50, 20{,}3)$
Part 13 to 14	$trans(0, 0, 85)$

After 3D HTM calculation, the nominal position in X, Y, Z axes are 649,99mm, 616,52mm and 57,68mm. Only Z axis has 0,18mm difference due to the dimension error in Z axis in Creo assembly measurement. However, this error is not big enough to influence the final results.

When the 3D HTM calculation results match Creo results in the nominal distance, the methods to analyze the tolerance variation need to be figured out. In a 3D problem, both the tolerance variation from the axes translation and the axes angle rotation must be accounted for in each transformation.

The RSS method has been chosen to calculate the axes translation error. Table 4 shows the formula we used to calculate the axes angle rotation error. It is based on the axes translation error and axes nominal distance.

Table 4 Angle rotation error calculation methods.

X axis angle rotation error	
Y≠0, Z=0 (nominal distance)	ATAN (Z axis tolerance translation error/ Y axis nominal distance) *180/PI ()
Y=0, Z≠0 (nominal distance)	ATAN (Y axis tolerance translation error / Z axis nominal distance) *180/PI ()
Y≠0, Z≠0 (nominal distance)	Minimum value between ATAN (Z axis tolerance translation error / Y axis nominal distance) *180/PI () and ATAN (Y axis tolerance translation error / Z axis nominal distance) *180/PI ()
Y axis angle rotation error	
X≠0, Z=0 (nominal distance)	ATAN (Z axis tolerance translation error / X axis nominal distance) *180/PI ()
X=0, Z≠0 (nominal distance)	ATAN (X axis tolerance translation error / Z axis nominal distance) *180/PI ()
X≠0, Z≠0 (nominal distance)	Minimum value between ATAN (Z axis tolerance translation error / X axis nominal distance) *180/PI () and ATAN (X axis tolerance translation error / Z axis nominal distance) *180/PI ()

Z axis angle rotation error	
X≠0, Y=0 (nominal distance)	ATAN (Y axis tolerance translation error / X axis nominal distance) *180/PI ()
X=0, Y≠0 (nominal distance)	ATAN (X axis tolerance translation error / Y axis nominal distance) *180/PI ()
X≠0, Y≠0 (nominal distance)	Minimum value between ATAN (Y axis tolerance translation error / X axis nominal distance) *180/PI () and ATAN (X axis tolerance translation error / Y axis nominal distance) *180/PI ()

The final step is to calculate the distance variation between the part 9 pin tip and part 14 top surface center. This calculation needs to be done using Crystal Ball software to run a Monte Carlo Simulation. The simulation results will be presented in chapter 4.3. Before that, every axes translation and angle rotation error inside every transformation needs to be figured out.

There are three types of variations as mentioned in chapter 2.1.6.. According to these three types of variation, all the possible errors between the parts and joints can be found out. For example, from part 1 to part 2 transformation one joint is included. Table 5 shows the errors from part 1 to part 2 in X, Y and Z axes direction.

Table 5 X, Y and Z axes direction variation elements.

	Variation elements
X direction	X axis dimensional variation.
	The joint variation which is hole allowance from part 1 and the screw hole allowance from part 2.
	X axis angle rotation variation.
Y direction	Y axis dimensional variation.
	The joint variation which is hole allowance from part 1 and the screw hole allowance from part 2.

	Y axis angle rotation variation.
Z direction	Surface flatness in part 1
	Surface flatness in part 2
	Z axis angle rotation variation.

4.2 *Analysis of 3D scanning data*

3D scanning the parts were carried out by two different 3D optical scanners called GOM Atos Triple Scan and Atos Core. Atos Core scanned over 200mm parts and smaller than 200mm parts measurements were carried out by Atos Triple scanner showed in Figure 34. Both scanners were set to 20° as the measuring temperature. A total of 12*5 parts were scanned. In detail there were 12 parts and every part had five series. These 12 parts are critical for the loop chain diagram analysis. All the parts were fixed on the rotary table using black plasticine.

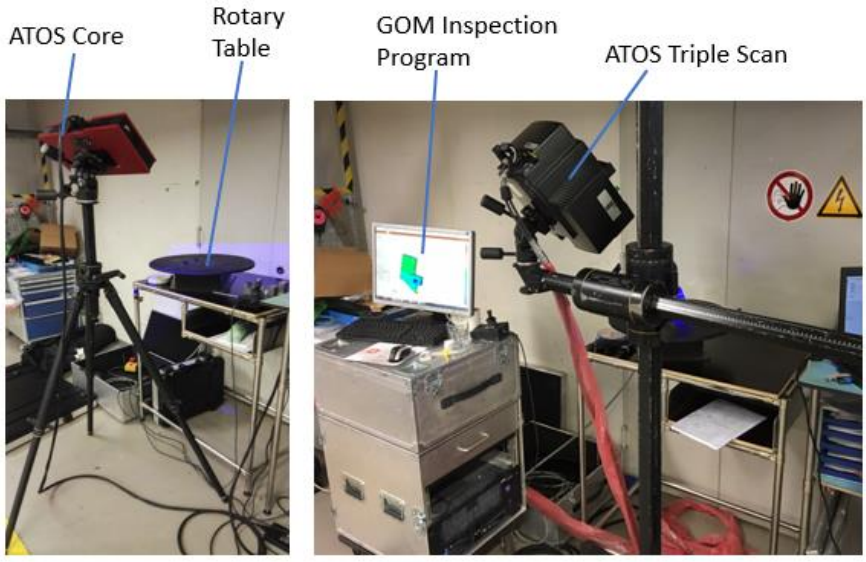

Figure 34 3D scanning parts configuration.

3D scanning the whole assembled device also used Atos Triple scan and Atos Core showed in Figure 35. Atos Triple Scan was used to scan the outline of the whole assembly machine. Atos Core was used after the Atos Triple Scan to scan the details of the whole assembled

device. Atos Triple scanner was set to 22° and Atos Core was set to 20° as measuring temperature. There were a total of five series of the assembled machine. All five devices were assembled using the previously scanned parts.

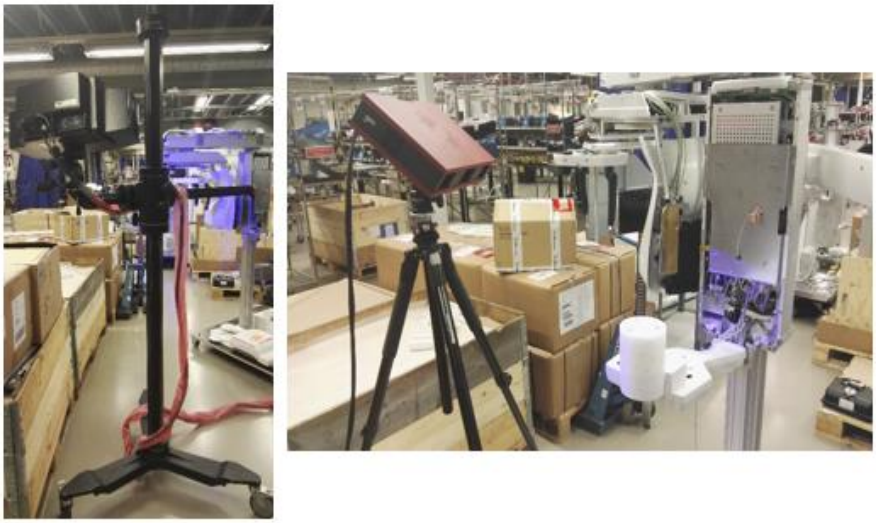

Figure 35 3D scanning assembly configuration.

3D scanning measurement data were gotten from GOM Inspect program. Figure 36 and 37 illustrate 3D scanning image of part 1 and the assembled device in GOM Inspect program. A comparison between the 3D scanning product and CAD model is shown in Figure 38. Nominal dimension means the dimension from the CAD model and Actual means dimension from the 3D scan. There were some errors introduced from the GOM program measurement or during the 3D scanning process. For example, 3D scanning cannot get a good surface image from the screw hole, therefore no screw hole allowances were measured.

During the scanning process, the scanner lights and the angle to scan the parts needs to be adjusted manually. Additionally, all reflective surfaces on parts need to be sprayed to lower the surface lightness. These steps can heavily increase the time required for the 3D scanning process. Based on these requirements, the two 3D scanners used in this thesis project are not suitable for large batch continuous scanning operations such as in the production line to inspect incoming goods quality. They are mainly suited for scanning a small number of products and so would be more suitable for use in product development.

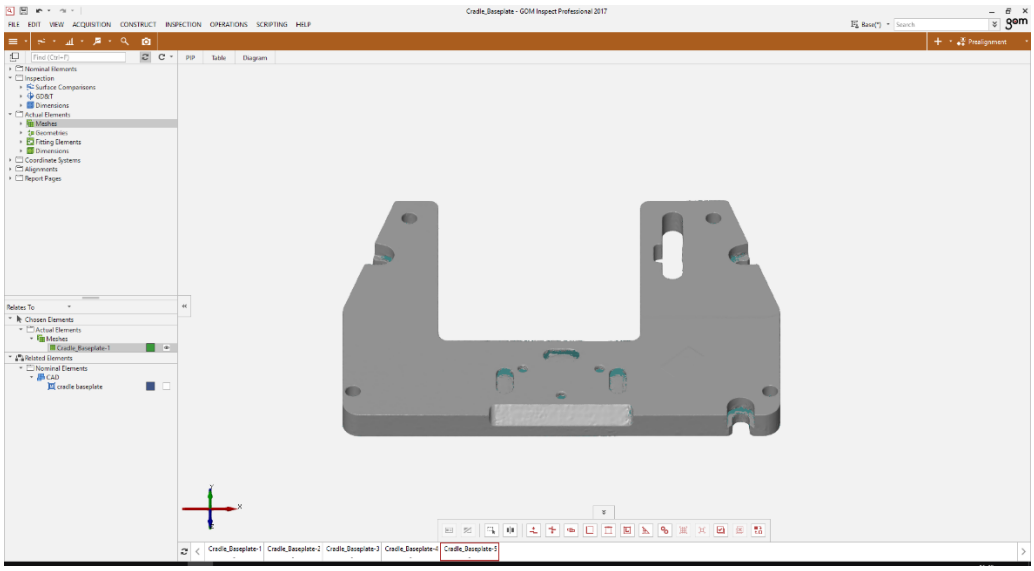

Figure 36 Part 1 3D scanning image.

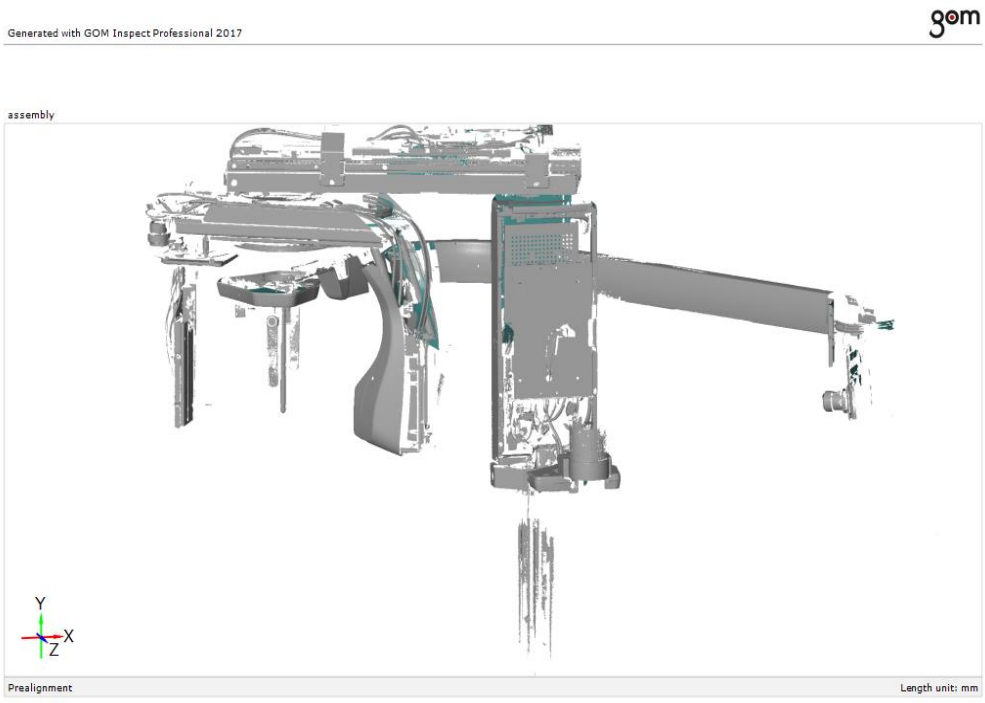

Figure 37 Assembly machine 3D scanning image

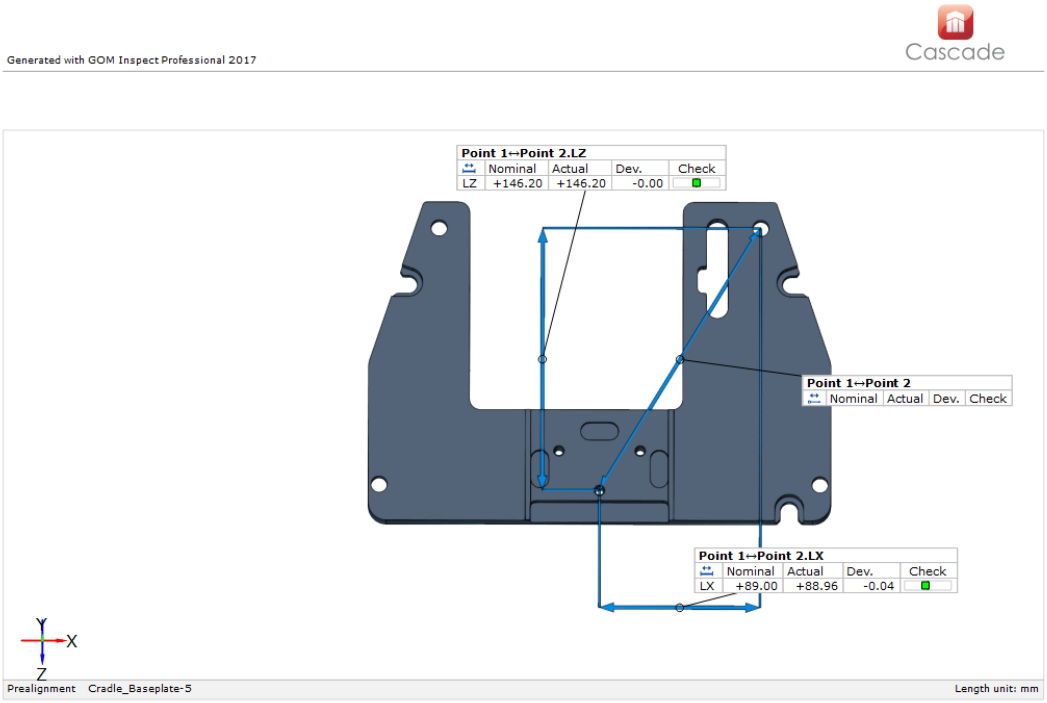

Figure 38 Part 1 CAD model and 3D scanning comparison results.

The 3δ value was obtained from 3D scanning parts measurement data. It represents the parts tolerance variation in reality. Comparing the defined tolerance in CAD drawing to the 3δ value can be used to inspect product quality efficiently. Figure 39 shows the ratio between the measured tolerance and the defined tolerance. There were nine measured tolerances that were two times bigger than the defined tolerance and among them, two were over 700%.

Nine measured values were checked for errors, and three out of nine measured tolerances had a measurement error. One of five sample data varied far more than the other sampled values. When getting rid of this one error, 3δ value decreased significantly. In total, only six measured tolerances were twice over the defined tolerance and two of them were over 700%.

From 3D scanning the whole assembled device measurement data, in X, Y and Z axes the distance variation between part 9 pin tip and part 14 top surface center were 8,9mm, 5,5mm and 5,5mm. According to Table 6, the X and Y axes distance variation between part 9 pin tip and part 14 top surface center met the performance requirement in production assembly.

From the 3D scanning data, we know that the defined tolerance was too tight. Nearly 34% of measured dimensions were over the defined tolerance, but the final assembly results were still within the performance requirements.

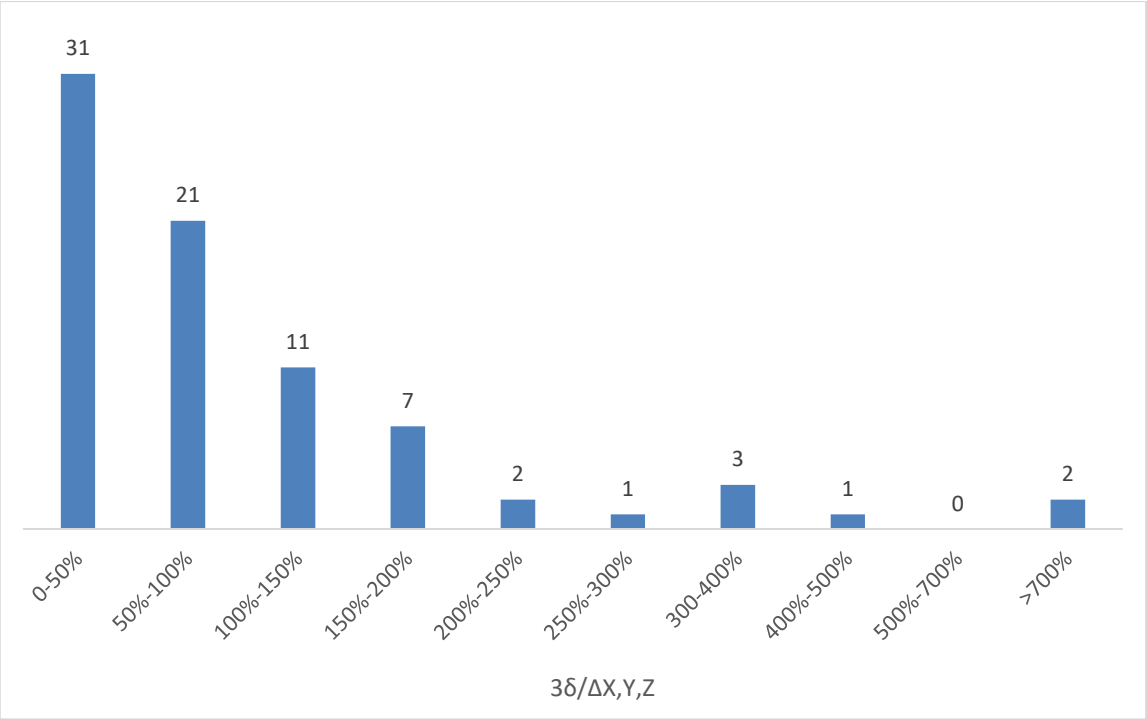

Figure 39 Measuring data 3δ tolerance value over the defined tolerance value.

Table 6 Part 9 to Part 14 3D scanning X, Y, Z Axes distance variation.

Total position	3δ (mm)
X	8,904
Y	5,508
Z	5,580

4.3 *Crystal Ball Monte Carlo tolerance analysis*

Tolerance analysis was done with Crystal Ball software. Monte Carlo simulations were based on HTM calculator in Microsoft Excel. Crystal Ball is a Microsoft Excel-based software tool. It is popular for simulation, forecasting and optimization. From chapter 4.1 and chapter 4.2, we derived all the tolerance values from the theoretical calculation and 3D scanning measurement. The next step is to input all those data into two separate HTM calculator sheets.

Table 7 shows the example of HTM input data. Tolerance value needs to be put in USL column. The LSL is the same value as USL but with a negative sign. The column marked as green is the area where the Crystal Ball software is doing the Monte Carlo simulation. It

picks the random number from LSL and USL. Each simulation has 1,000,000 runs to ensure the accuracy of the results.

Table 7 HTM input data example.

Axis 1

	Nominal Location	Location Error		LSL	USL
X axis rotation. (deg)	0	ex (deg)	0	-0,166	0,166
Y axis rotation. (deg)	0	ey (deg)	0	-0,273	0,273
Z axis rotation. (deg)	0	ez (deg)	0	-0,142	0,142
X axis translation	89	dx	0	-0,361	0,361
Y axis translation	146,2	dy	0	-0,539	0,539
Z axis translation	0	dz	0	-0,424	0,424

After simulation, the results were presented with distribution charts and sensitivity charts. Distribution charts represent the error from part 1 to part 9 and from part 14 to part 1 in X, Y, Z axes and RMS Total Position. Sensitivity charts represent which parts can cause serious error during assembly in X, Y, Z axes and RMS Total Position.

Figure 40 shows the Monte Carlo simulation distribution chart. It predicted that the X axis from part 9 to 14, the maximum error variation during assembly was about 200mm. For the 3D scanning measured error variation the value was 8,9mm in the X axis. There was the same situation with Y, Z axes and RMS Total position as shown in Table 8. The predicted value is far greater than the measured value. The huge difference is most likely due to jigs and assembly instructions to decrease the error rather than contributing it. The Monte Carlo simulation represents the worst case assembly process.

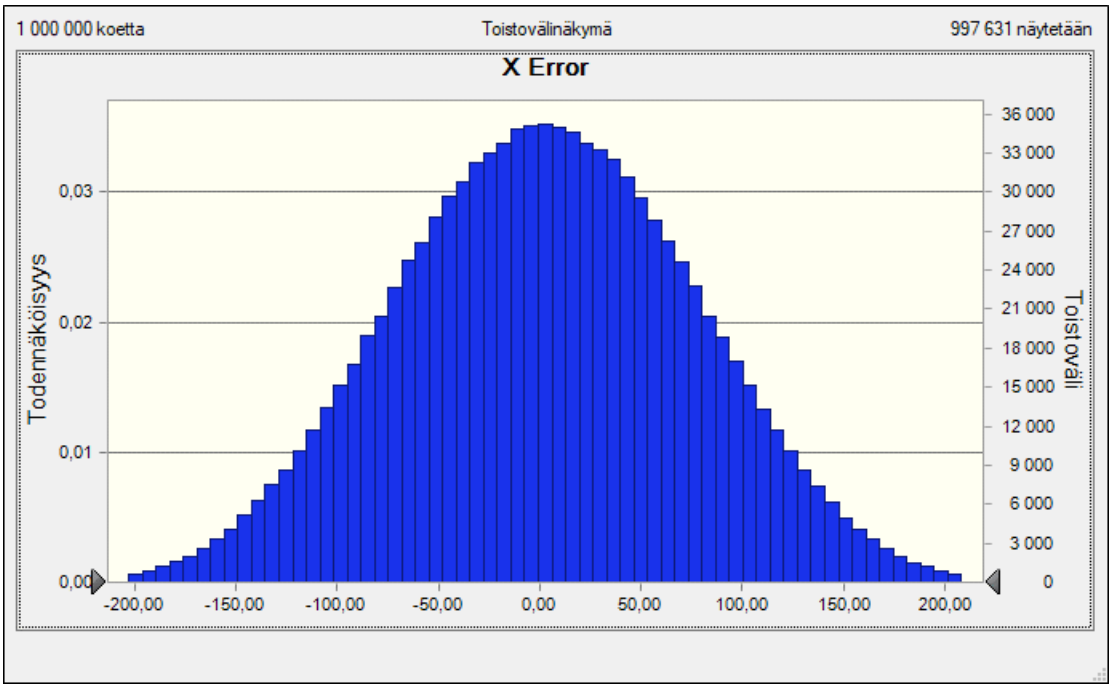

Figure 40 X axis error distribution chart in 3D scanning measurement data.

Table 8 Simulation results

	Distance variation (mm)
Total position from parts 9 tip to top surface center part 14	
X axis	±200
Y axis	±200
Z axis	-90 to120
RMS Total position	0 to 240

Table 9 shows the sensitivity analysis results in X axis for both 3D scanning 3δ tolerance value and the theoretical tolerance value. The first contributor always has the biggest influence in X axis error. From the top four contributors, the ranking with each contributor in 3D scanning and theoretical tolerance value is different, but they have all the same contributors aside from the third one.

Table 9 Sensitivity analysis results in X axis.

	3D scanning 3δ tolerance value	theoretical tolerance value
First Contributor	Y axis rotation, from part 10 to 11	Y axis rotation, from part 11 to part 12
Second Contributor	Y axis rotation, from part 12 to 13	Y axis rotation, from part 10 to 11
Third Contributor	Z axis rotation, from part 1 to part 10	Y axis rotation, from part 1 to part 10
Fourth Contributor	Y axis rotation, from part 11 to part 12	Y axis rotation, from part 12 to 13

Table 10 shows the sensitivity analysis results in Y axis for both 3D scanning 3δ tolerance value and the theoretical tolerance value. The top two contributors influencing both the Y axis error in 3D scanning and theoretical tolerance value are the same. From the third contributor to the seventh contributor, the ranking is different, but they have nearly the same contributors.

Table 10 Sensitivity analysis results in Y axis.

	3D scanning 3δ tolerance value	theoretical tolerance value
First Contributor	X axis rotation, from part 3 to part 4	X axis rotation, from part 3 to part 4
Second Contributor	Z axis rotation, from part 3 to part 4	Z axis rotation, from part 3 to part 4

Table 11 shows the sensitivity analysis results in Z axis for both 3D scanning 3δ tolerance value and the theoretical tolerance value. The top one contributor influencing Z axis error in 3D scanning and theoretical tolerance value is the same. From the second contributor to the seventh contributor, the ranking is different but they have the same contributors.

Table 11 Sensitivity analysis results in Z axis.

	3D scanning 3δ tolerance value	theoretical tolerance value

First Contributor	Y axis rotation, from part 3 to part 4	Y axis rotation, from part 3 to part 4
Second Contributor	X axis rotation, from part 3 to part 4	Y axis rotation, from part 4 to part 5

Table 12 shows a sensitivity analysis results in RMS total position for both 3D scanning 3δ tolerance value and the theoretical tolerance value. The top one contributor is not the same in 3D scanning and theoretical tolerance value but within the same parts transformation.

Table 12 Sensitivity analysis results in RMS Total position.

	3D scanning 3δ tolerance value	theoretical tolerance value
First Contributor	X axis rotation, from part 10 to part 11	Y axis rotation, from part 10 to part 11

To determine which parts are the most sensitive in X, Y and Z axes we put all the tolerance values to 0,1 and run the Monte Carlo simulation again. Table 13 shows the results of the sensitive parts in X, Y and Z axes.

Table 13 Sensitive parts in X, Y, Z axes.

X axis	
First	Z axis rotation, from part 10 to part 11
Second	Y axis rotation, from part 1 to part 10
Y axis	
First	Y axis rotation, from part 4 to part 5
Second	Z axis rotation, from part 2 to part 3
Z axis	
First	Y axis rotation, from part 4 to part 5

Second	X axis rotation, from part 5 to part 6

Comparing the simulation results between 3D scanning and theoretical tolerance value, the most critical parts in X, Y and Z axes are nearly the same. Without the 3D scanning data and assuming everything within the defined tolerance range, the theoretical simulation results are reliable. We need to pay attention to the sensitive parts even though they are not the biggest problem to cause axes error.

5 Solution

From the last chapter, we already know which parts are important to X, Y and Z axes error. Solutions need to be found to reduce their influence on the whole assembly. Each simulation result has 5000 runs. The solution is based on the 3D scanning 3δ tolerance value.

5.1 *X axis error*

According to Table 9, the first contributor in X axis error is Y axis rotation, from part 10 to 11. According to table 4, Y axis rotation error depends on X and Z axes translation error.

Table 14 Part 10 to part 11 X and Z axes translation error.

		defined tolerance	3D scanning 3δ tolerance	
ΔX	x axis dimensional tolerance	±0,1	±0,091	91,49 %
	slot hole on part 10	±0,26	±0,203	78,00 %
	guiding feature hole on part 11	±0,08	±0,087	109,33 %
ΔZ	Z axis dimensional tolerance	±0,15	±0,250	166,53 %

Z axis translation error from part 10 to 11 is nearly 1,5 over the defined tolerance value shows in Table 14. Decreasing this number to original 0,15mm, the biggest contributor did not change. Continue decreasing it until 0,05mm, then the results are getting better. It is in third place.

In X axis translation error, there are three variation issues included. 3D scanning tolerance value of the guiding feature hole on part 11 is a little bit bigger than defined tolerance. Decreasing the 3D scanning tolerance value to 80% of defined tolerance. The Y axis rotation, from part 10 to 11 are in fourth place. Table 15 below shows the best solution for the first contributor in X axis error.

Table 15 Best solution for Y axis rotation, from part 10 to 11 in X axis error.

		tolerance value
ΔX	x axis dimensional tolerance	±0,091
	slot hole on part 10	±0,203
	guiding feature hole on part 11	±0,064
ΔZ	Z axis dimensional tolerance	±0,050

The second contributor in X axis error is Y axis rotation, from part 12 to 13. According to table 4, Y axis rotation error depends on X and Z axes translation error.

Table 16 Part 12 to part 13 X and Z axes translation error.

		defined tolerance	3D scanning 3δ tolerance	
ΔX	gap between part 12 and part 13	±0,2	±0,225	112,55 %
ΔZ	Z axis dimensional tolerance	±0,2	±0,347	187,17 %
	surface flatness on part 12	0-0,5	0-0,5	100 %
	surface flatness on part 13	0-0,5	0-0,5	100 %

Z axis dimensional tolerance is nearly twice as large as defined tolerance shows in Table 16. Decreasing Z axis dimensional tolerance to original ±0,2mm Y axis rotation, from part 12 to 13 is still the biggest contributor. However, further decreasing the Z axis dimensional tolerance to 0, the results did not change at all. Z axis dimensional tolerance is not the issue influencing the results.

X axis translation error is over the defined tolerance value. Reducing the tolerance value from the gap between part 12 and part 13 to original ±0,2mm the results did not change.

Further decreasing the tolerance to 60% of the defined tolerance, the Y axis rotation, from part 12 to 13 is in third place. Were it possible to change both surface flatness tolerance on part 12 and part 13 to 0,3mm, the result would be in fifth place.

Table 17 Best solution for Y axis rotation, from part 12 to 13 in X axis error.

		tolerance value
ΔX	gap between part 12 and part 13	±0,12
ΔZ	Z axis dimensional tolerance	±0,347
	surface flatness on part 12	0 to 0,3
	surface flatness on part 13	0 to 0,3

5.2 *Y axis error*

According to Table 10, the first contributor in Y axis error is X axis rotation, from part 3 to 4. According to table 4, X axis rotation error depends on Y axis translation error.

Table 18 Part 3 to part 4 Y axis translation error.

		defined tolerance	3D scanning 3δ tolerance	
ΔY	Y dimension tolerance	±0,2	±0,148	73,79 %
	surface flatness on part 3	0 to 0,3	±2,546	848,81 %
	surface flatness on part 4	0 to 0,3	±0,564	187,88 %

According to Table 18, surface flatness tolerance on part 3 is eight times over the defined tolerance. Decreasing this value to original ±0,3mm the result is still the same. Further reducing the surface flatness on part 3 to 0, the result still did not change. Changing both surface flatness on part 3 and part 4 to 80% of the original defined tolerance value the X axis rotation from part 3 to 4 become the second contributor. Further decreasing both surface flatness tolerance values to 0 the result is in the third place. All manufactured parts have tolerance, making this situation impossible in reality. When the surface flatness tolerance

value changes, the result of Y axis error did not change, but the percentage in the whole sensitivity chart changes. Table 19 shows the best solution for the first contributor in Y axis error.

Table 19 Best solution for X axis rotation, from part 3 to 4 in Y axis error.

		tolerance value
ΔY	Y dimension tolerance	±0,148
	surface flatness on part 3	0 to 0,21
	surface flatness on part 4	0 to 0,21

The second contributor in Y axis error is Z axis rotation, from part 3 to 4. According to table 4, Z axis rotation error also depends on Y axis translation error. When dealing with the first contributor, the best solution is also useful in the second contributor. The results of Z axis rotation, from part 3 to 4 is in fifth place.

The third contributor in Y axis error is Y axis rotation, from part 6 to 7. It has the most share in the sensitivity chart after solving the first and second contributors. According to table 4, Y axis rotation error depends on Z axis translation error.

Table 20 Part 6 to part 7 Z axis translation error.

		defined tolerance	3D scanning 3δ tolerance	
ΔZ	Z dimension tolerance	±0,3	±0,109	36,47 %
	hole distance on part 7	±0,2	±1,454	727,04 %

According to Table 20, hole distance on part 7 is seven times over the defined tolerance. Decreasing it to original ±0,2mm the Z axis rotation from part 3 to 4 has the best results is in sixth place.

5.3 *Z axis error*

According to Table 11, the first contributor in Z axis error is Y axis rotation, from part 3 to 4. According to table 4, Y axis rotation error depends on X axis translation error.

Table 21 Part 3 to part 4 X axis translation error.

		defined tolerance	3D scanning 3δ tolerance	
ΔX	X axis dimension tolerance	±0,2	±0,324	162,11 %
	slot hole on part 4	±0,2	±0,288	144,11 %
	Screw hole on part 3	±0,022	±0,03	136,36%

All the 3D scanning tolerance are over the defined tolerance in the drawing shown in Table 21. Screw hole cannot be measured accurately using 3D scanning due to its shape and depth. Based on information from manufacturing industry we can assume all the screw hole tolerances to be ±0,03mm. This tolerance is larger than the defined tolerance in the drawing. When changing all the tolerance to original defined value, the result is still the same. Until we decrease X axis dimension and slot hole on part 4 tolerance value to half of the defined value, the result of Y axis rotation, from part 3 to 4 is in third place. Table 22 shows the best solution.

Table 22 Best solution for Y axis rotation, from part 3 to 4 in Z axis error.

		tolerance value
ΔX	X axis dimension tolerance	±0,1
	slot hole on part 4	±0,1
	Screw hole on part 3	±0,03

The second contributor in Z axis error is X axis rotation, from part 3 to 4. When dealing with Y axis rotation error from part 3 to 4, the Z axis error result already changed to fourth place. The Current second contributor is Y axis rotation, from part 4 to 5.

Table 23 Part 4 to part 5 X axis translation error.

		defined tol-erance	3D scanning 3δ tolerance	
ΔX	X axis dimension tol-erance	±0,2	±0,214	107,03 %
	hole on part 4	±0,2	±0,202	100,85 %
	Slot hole on part 5	±0,2	±0,2	100%

According to Table 23, X axis dimension tolerance and hole on part 4 tolerance are a little bit over the defined value. Decreasing both values to original defined tolerance values will not make any changes for the result. Further lowering both tolerance values to 0, the Y axis rotation from part 4 to 5 rises to second place. This situation could not happen in reality. The results are the same when decreasing all the tolerances to 80% of defined tolerance. Even decreasing until 10% of the defined tolerance, the value of the Y axis rotation from part 4 to 5 is still in the second place, but the percentage in sensitivity charts become smaller and smaller. Table 24 shows the best solution for the second contributor in Z axis error.

Table 24 Best solution for X axis rotation, from part 4 to 5 in Z axis error.

		tolerance value
ΔX	X axis dimension tolerance	±0,16
	hole on part 4	±0,16
	Slot hole on part 5	±0,16

6 Future research

Many research areas remain open after the conclusion of this research project. Inclusion of material deformation in the tolerance analysis model could potentially increase the accuracy of simulation results significantly as they seemed to contribute to the realized results in the tolerances. Application of tolerance analysis results to ensure high quality assembled products in production assembly could be further researched with highly practical implications for industrial application. Further research on differences between computer-aided tolerance software, such as CETOL, VisVSA and 3DCS , and the utilized methods' impact on the resulting simulation could hold vastly more practical meaning than assumed for this project. There also exists many alternative methods for product quality inspection than 3D scanning where both qualitative and quantitative comparison between methods is needed. Further implications of the wider supply chain and suppliers' effect on product tolerance should also be considered holistically for a thorough understanding of tolerance analysis as it is applied in industrial settings

Additional topics also remain in the field of tolerances aside from those already discussed for tolerance analysis in particular. The traditional approach to mechanical tolerancing follow the flow of moving from requirements elicited from the customer to the manufacturing shop floor. The full process flow is shown below: (Drake, 1999)

- The requirements from the customer forms the design specification.
- A system engineering separates the design specifications in different disciplines such as mechanical design, electrical design and software design.
- The subassemblies within mechanical design get the mechanical design requirements.
- The parts within subassembly get the requirements from mechanical subassembly.
- The manufacturing shop get the parts dimensional and tolerancing requirements.

The biggest drawback in this flow is that we find out only at the end of the endeavor whether the manufacturing process can make the required parts meet the tolerance well. This in effect makes customer requirements more difficult to achieve. This process flow could also prove more prone to producing less cost-effective parts as customer requirements are only captured at the beginning and tolerances are matched to these requirements after the fact. To facilitate

these challenges and as an extension of this process we can add the manufacturing requirements as an input to the design process. The suggested revisions to the process are shown below: (Drake, 1999)

- The manufacturing requirements are defined for the parts. If we know the variation of the parts manufacturing process, we can calculate the variation of the parts' features.
- The parts' feature variations are used as inputs to the subassembly.
- From subassembly variation we can determine the variation for the whole mechanical system.
- With mechanical system variation at hand we can determine the probability of meeting the customer requirements.

The key benefit of this revised process is the early establishment of the expected part performance and design risk. This process doesn't use tolerance to drive manufacturing but instead uses manufacturing machine capability to drive design. (Drake, 1999). The application of the revised design process flow has been introduced in research literature but its practical application hasn't been sufficiently researched. If mechanical tolerancing in industrial settings were to follow the new approach what implications would this have for tolerance analysis?

7 Summary

In this thesis, the tolerance analysis process was developed in the context of a 3D design. HTM was adopted to describe every parts' relative position in the assembly process. Based on the HTM model, Crystal Ball analytical software was used to run Monte Carlo simulations and complete a tolerance analysis. The distribution charts and sensitivity charts from the simulation results were used to help understand every individual component variation and the complete assembly process of a dental X-ray machine. 3D scanning is a new development area in KavoKerr. This technology is widely used in the industrial field in product quality inspection and reverse engineering. In this research, 3D scanning was used to inspect product quality. This research also worked as a trial for 3D scanning technology and provided valuable suggestions to KavoKerr for the future application of 3D scanning technology.

Based on a literature review of the tolerance analysis process, six steps were identified to perform a tolerance analysis. The first step was to consider the performance requirements which in this research was determined to be a distance variation within ±10mm from assembly part 9 to part 14. The second step taken was to create a loop diagram. This research was focused on 3D tolerance analysis so the resulting loop diagram was also 3D. The third step was to transfer all the dimension to equal bilateral dimension. The fourth step was to calculate the mean dimension of performance requirements. HTM was used to calculate the nominal distance from part 9 and part 14. The X, Y and Z axes nominal dimensions calculated using HTM should then be the same as the measured dimensions in a Creo model. In a few instances a small error between HTM calculated and Creo measured dimension was observed and was identified to be caused by Creo assembly error. It proved difficult to match three dimensions exactly. Given that this error was small enough to pose minimal influence on the final results the nominal dimension in HTM was used to do the tolerance analysis. The fifth step was to decide the calculation method for tolerance analysis. In 3D tolerance analysis, the error contains translation error and angle rotation error. The RSS method was used to calculate the translation error while angle rotation error was calculated based on the nominal dimension and the translation error. The final step was to calculate the variation of performance in part requirements.

The tolerance analysis results can be obtained from running Monte Carlo simulations. Crystal Ball Monte Carlo simulation was used to get the distance variation results from part 9 to

part 14. 1 million simulation runs of both the 3D scanning measured data and the defined tolerances in drawings was used in order to ensure accuracy in the results. Distribution charts were generated and represent the distance variation from part 9 to part 14. The results based on the 3D scanning measured data in the simulation distribution charts for the X, Y and Z axes were ±200mm, ±200mm and -90 to +120mm respectively. In 3D scanning the observed distance variation from part 9 to part 14 in X, Y and Z axes was ±8,9mm, ±5,5mm and ±5,5mm respectively. The simulated results and 3D scanning results clearly had a huge difference. The determined cause of this difference were the quality increasing practices in the assembly process, where jigs and assembly instructions were used to decrease the error rather than contributing it. The simulation results could then be taken to be a kind of a worst-case result obtainable given no process-based error mitigation. The distribution chart results were not reliable compared to the 3D scanning measured data. The sensitivity charts represent the parts' different contribution levels to X, Y and Z axes error as well as RMS total position error. The chart assists in determining which parts in whole assembly process are most important in terms of error contribution. In X axis error, the biggest contributor for 3D scanning measurement data and defined tolerance data was Y axis rotation from part 10 to 11 and Y axis rotation from part 11 to 12. In Y axis error, the biggest contributor for both simulations was X axis rotation from part 3 to part 4. In Z axis error, the biggest contributor for both simulations was Y axis rotation from part 3 to part 4. In RMS total position error, the biggest contributor for 3D scanning measurement data and defined tolerance data was X axis rotation from part 10 to part 11 and Y axis rotation from part 10 to part 11. The sensitivity chart results were similar for both the 3D scanning measured tolerance data and the defined tolerances in the drawing. When the sensitivity chart results are different for defined and simulated tolerances the clear implication is that the parts tolerance is over the defined tolerance. It is then important to correct the tolerance value to within the defined tolerance range.

Two different types of models of 3D optical scanners were used in this research for parts and assembly device scanning. During part scanning 12 distinct parts with 5 samples of each were scanned. For the assembly device scanning a total of 5 series of devices were scanned. Both scanners needed to be warmed up to a certain temperature before use. Adjustment of camera lighting and reference point stickers was experienced to be important for scanning result accuracy. These points assist in taking a good quality picture and helped subsequent

bundling of all the single scanned pictures together. Occasionally getting a good quality picture out of the scanners was experienced to take a long time as the scanners were very sensitive to positional movement. Quality of the scanned picture was observed to be of vital importance as it directly affected the accuracy of the measured dimensions. GOM Inspection program was used to measure the dimension between the CAD model and 3D scanning parts.

As an outcome of this research, the utilized 3D scanning methods were determined not to be suited for the production line for large batch operations. The method was helpful in checking a small quantity of products and in measuring dimensions where traditional methods were difficult to use. In the particular assembly device tested in this research some of the parts had to be sprayed to lower the surface shine. This in part contributed to the added effort when doing the 3D scanning. From the 3D scanning results, nearly 34% of measured tolerance was over defined tolerance but the distance variation for X, Y and Z axes all still met the performance requirements for the parts, which were within ±10mm. It was found that the currently defined tolerances for the assembly device in the drawing were a bit too tight and should be loosened.

The biggest challenge in this research was figuring out every transformations 3D nominal position in the loop diagram and getting the HTM calculation working. When the loop diagram changes, the whole tolerance analysis will have to change respectively necessitating a start from the beginning. In the HTM calculator sheet used for analysis there was a large amount of data that had to be collected in every transformation nominal position and tolerance value. Nominal position of every transformation was not easy to match with the HTM calculated final results. Developing a process to use a 3D scanner to get a good scanning image out of a physical product was also a non-trivial task.

List of references

Abdel-Bary Ebrahim, M. (2011) '3D Laser Scanners: History, Applications, and Future', (October 2014), pp. 1–81. doi: 10.13140/2.1.3331.3284.

Arras, P. and Merode, D. Van (2012) 'DIMENSIONAL TOLERANCE ANALYSIS OF DESIGNS IN MECHANICAL CADSYSTEMS Abstract : Introduction ':, *Acta Technologica Agricultura*, 12(4), pp. 93–95.

ATOS Triple Scan – Industrial Optical 3D Digitizer (no date) *GOM*. Available at: https://www.gom.com/metrology-systems/atos/atos-triple-scan.html.

Bernd, B. (2014) '25 years of High Definition 3D Scanning: History, State of the Art, Outlook', *Electronic Visualisation and the Arts (EVA 2014)*. Available at: http://dx.doi.org/10.14236/ewic/eva2014.31.

Botero, V. J. S., Hernández, W. and Fernández, E. (2014) 'Orientation of a triaxial accelerometer using a homogeneous transformation matrix and Kalman filters', *International Journal on Smart Sensing and Intelligent Systems*, 7(4), pp. 1631–1646.

Brajlih, T. *et al.* (2011) 'Possibilities of Using Three-Dimensional Optical Scanning in Complex Geometrical Inspection', *Strojniški vestnik – Journal of Mechanical Engineering*, 57(11), pp. 826–833. doi: 10.5545/sv-jme.2010.152.

Bryan Dodson, Patrick Hammett, Rene Klerx, and R. K. (2014) *Probabilistic Design for Optimization and Robustness for Engineers*. John Wiley & Sons, Incorporated. Available at: https://ebookcentral.proquest.com/lib/aalto-ebooks/detail.action?docID=1744260.

Chase, K. W. (1999) *Tolerance Analysis of 2-D and 3-D Assemblies (Automated Method)*. Available at: http://adcats.et.byu.edu/Publication/99-4/MultiDimTolAssem.pdf.

Chen, H. *et al.* (2014) 'A comprehensive study of three dimensional tolerance analysis methods', *CAD Computer Aided Design*. Elsevier Ltd, 53, pp. 1–13. doi: 10.1016/j.cad.2014.02.014.

Drake, P. J. (1999) *Dimensioning and Tolerancing Handbook*. McGraw-Hill. Available at: http://books.google.com.co/books?id=XOxqQgAACAAJ.

Engineering & Manufacturing Services (2017) *Types of 3D Scanners and 3D Scanning Technologies* .

Funke, C. (2016) 'GOM 3D Metrology Systems'. Available at: http://www.k3works.de/fileadmin/user_upload/News/005_presentation_optical_measurement.pdf.

Gao, J., Chase, K. W. and Magleby, S. P. (1998) 'Generalized 3-D tolerance analysis of mechanical assemblies with small kinematic adjustments', *IIE Transactions (Institute of Industrial Engineers)*, 30(4), pp. 367–377. doi: 10.1080/07408179808966476.

Kuş, A. (2009) 'Implementation of 3D optical scanning technology for automotive applications', *Sensors*, 9(3), pp. 1967–1979. doi: 10.3390/s90301967.

Laing, L. W. W. (1994) ‘An introduction to 3D Scanning’, *Computer-Aided Design*, 26(2), pp. 157–158. doi: 10.1016/0010-4485(94)90038-8.

Lin, E. E. and Zhang, H. C. (2001) ‘Theoretical tolerance stackup analysis based on tolerance zone analysis’, *International Journal of Advanced Manufacturing Technology*, 17(4), pp. 257–262. doi: 10.1007/s001700170178.

Tolerance Stack-Up Analysis (no date) *Technical Training consultants*. Available at: http://www.ttc-cogorno.com/Newsletters/140117ToleranceAnalysis.pdf (Accessed: 30 July 2018).

Varady, T., Martin, R. R. and Cox, J. (1997) ‘Reverse engineering geometric models-an introduction’, *Computer Aided Design*, 29(4), pp. 255–268.

Whitney, D. E. (2004) *Mechancial Assemblies Their deaign, Manufacuture, and Role in Product Development*. Edited by J. R. Crookall, M. C. Shaw, and N. P. Suh. Oxford University Press, Inc. Available at: http://alvarestech.com/temp/PDP2011/Texto/Mechanical Assemblies Their Design Manufacture and Role in Product Development.pdf.

List of appendices

Appendix 1. HTM calculator Excel sheet.

Appendix 2. X axis sensitivity charts of defined tolerance in drawing.

Appendix 3. Y axis sensitivity charts of defined tolerance in drawing.

Appendix 4. Z axis sensitivity charts of defined tolerance in drawing.

Appendix 5. RMS axis sensitivity charts of defined tolerance in drawing.

Appendix 6. X axis sensitivity charts of 3D scanning.

Appendix 7. Y axis sensitivity charts of 3D scanning.

Appendix 8. Z axis sensitivity charts of 3D scanning.

Appendix 9. RMS axis sensitivity charts of 3D scanning.

Appendix 1. HTM Calculator Excel Sheet

INPUTS:
First step: Calculate HTMs with all errors set to zero
Note: wrt = with respect to, CS = coordinate system, ref = reference, Loc = location, err = errors

Tool Axis 1 wrt ref CS

Loc		Loc Err		LSL	USL
X axis rot. (deg)	0	ex (deg)	0	-0,166	0,166
Y axis rot. (deg)	0	ey (deg)	0	-0,273	0,273
Z axis rot. (deg)	0	ez (deg)	0	-0,142	0,142
axis translation	89	dx	0	-0,361	0,361
axis translation	146,2	dy	0	-0,539	0,539
axis translation	0	dz	0	-0,424	0,424

Work Axis 1 wrt ref CS

Loc		Loc Err		LSL	USL
X axis rot. (deg)	0	ex (deg)	0	-0,065	0,065
Y axis rot. (deg)	0	ey (deg)	0	-0,419	0,419
Z axis rot. (deg)	0	ez (deg)	0	-0,551	0,551
X axis translation	-68	dx	0	-0,469	0,469
Y axis translation	-438	dy	0	-0,654	0,654
Z axis translation	4,06	dz	0	-0,498	0,498

Tool Axis 2 wrt tool CS 1

Loc		Loc Err		LSL	USL
X axis rot. (deg)	0	ex (deg)	0	-0,025	0,025
Y axis rot. (deg)	0	ey (deg)	0	0,000	0,000
Z axis rot. (deg)	0	ez (deg)	0	0,000	0,000
axis translation	0	dx	0	0	0
axis translation	14,5	dy	0	-0,2	0,2
axis translation	452	dz	0	-0,854	0,8544

Work Axis 2 wrt tool CS 1

Loc		Loc Err		LSL	USL
X axis rot. (deg)	0	ex (deg)	0	-4,086	4,086
Y axis rot. (deg)	0	ey (deg)	0	-0,648	0,648
Z axis rot. (deg)	0	ez (deg)	0	-7,858	7,858
X axis translation	13	dx	0	-0,290	0,290
Y axis translation	-2,1	dy	0	-0,290	0,290
Z axis translation	25,644	dz	0	-0,150	0,150

Tool Axis 3 wrt tool CS 2

Loc		Loc Err		LSL	USL
X axis rot. (deg)	0	ex (deg)	0	-0,744	0,744
Y axis rot. (deg)	0	ey (deg)	0	0,000	0,000
Z axis rot. (deg)	0	ez (deg)	0	-0,744	0,744
axis translation	0	dx	0	-0,201	0,2012
axis translation	15,5	dy	0	-0,469	0,469
axis translation	0	dz	0	-0,201	0,2012

Work Axis 3 wrt tool CS 2

Loc		Loc Err		LSL	USL
X axis rot. (deg)	0	ex (deg)	0	-0,490	0,490
Y axis rot. (deg)	0	ey (deg)	0	-0,882	0,882
Z axis rot. (deg)	0	ez (deg)	0	-0,200	0,200
X axis translation	55	dx	0	-0,369	0,369
Y axis translation	-105,9	dy	0	-0,369	0,369
Z axis translation	24	dz	0	-0,906	0,906

Tool Axis 4 wrt tool CS 3

Loc		Loc Err		LSL	USL
X axis rot. (deg)	0	ex (deg)	0	-4,470	4,470
Y axis rot. (deg)	0	ey (deg)	0	-2,707	2,707
Z axis rot. (deg)	0	ez (deg)	0	-1,120	1,120
axis translation	-24	dx	0	-0,284	0,2837
axis translation	7	dy	0	-0,469	0,469
axis translation	-6	dz	0	-0,225	0,2247

Work Axis 4 wrt tool CS 3

Loc		Loc Err		LSL	USL
X axis rot. (deg)	0	ex (deg)	0	-0,842	0,842
Y axis rot. (deg)	0	ey (deg)	0	-0,564	0,564
Z axis rot. (deg)	0	ez (deg)	0	-0,229	0,229
X axis translation	0	dx	0	-0,200	0,200
Y axis translation	50	dy	0	-0,361	0,361
Z axis translation	20,3	dz	0	-0,735	0,735

Tool Axis 5 wrt tool CS 4

Loc		Loc Err		LSL	USL
X axis rot. (deg)	0	ex (deg)	0		
Y axis rot. (deg)	0	ey (deg)	0		
Z axis rot. (deg)	-51	ez (deg)	0		
axis translation	0	dx	0		
axis translation	0	dy	0		
axis translation	0	dz	0		

Work Axis 5 wrt tool CS 4

Loc		Loc Err		LSL	USL
X axis rot. (deg)	0	ex (deg)	0	0,000	0,000
Y axis rot. (deg)	0	ey (deg)	0	0,000	0,000
Z axis rot. (deg)	0	ez (deg)	0	0,000	0,000
X axis translation	0	dx	0		
Y axis translation	0	dy	0		
Z axis translation	0	dz	0		

Tool Axis 6 wrt tool CS 5

Loc		Loc Err		LSL	USL
X axis rot. (deg)	0	ex (deg)	0	-0,744	0,744
Y axis rot. (deg)	0	ey (deg)	0	-2,496	2,496
Z axis rot. (deg)	0	ez (deg)	0	-0,367	0,367
axis translation	10,155	dx	0	-0,346	0,3464
axis translation	54,11	dy	0	-0,52	0,5196
axis translation	-40	dz	0	-0,412	0,4123

Work Axis 6 wrt tool CS 5

Loc		Loc Err		LSL	USL
X axis rot. (deg)	0	ex (deg)	0	0,000	0,000
Y axis rot. (deg)	0	ey (deg)	0	0,000	0,000
Z axis rot. (deg)	0	ez (deg)	0	0,000	0,000
X axis translation	0	dx	0		
Y axis translation	0	dy	0		
Z axis translation	0	dz	0		

Tool Axis 7 wrt tool CS 6

Loc		Loc Err		LSL	USL
X axis rot. (deg)	0	ex (deg)	0	-0,028	0,028
Y axis rot. (deg)	0	ey (deg)	0	-0,028	0,028
Z axis rot. (deg)	3	ez (deg)	0	-1,112	1,112
axis translation	-412,03	dx	0	-0,8	0,8
axis translation	-407,91	dy	0	-0,8	0,8
axis translation	21	dz	0	-0,2	0,2

Work Axis 7 wrt tool CS 6

Loc		Loc Err		LSL	USL
X axis rot. (deg)	0	ex (deg)	0	0,000	0,000
Y axis rot. (deg)	0	ey (deg)	0	0,000	0,000
Z axis rot. (deg)	0	ez (deg)	0	0,000	0,000
X axis translation	0	dx	0		
Y axis translation	0	dy	0		
Z axis translation	0	dz	0		

Tool Axis 8 wrt tool CS 7

Loc		Loc Err		LSL	USL
X axis rot. (deg)	0	ex (deg)	0	-1,830	1,830
Y axis rot. (deg)	0	ey (deg)	0	0,000	0,000
Z axis rot. (deg)	0	ez (deg)	0	-1,830	1,830
axis translation	0	dx	0	-0,224	0,2236
axis translation	-7	dy	0	-0,469	0,469
axis translation	0	dz	0	-0,224	0,2236

Work Axis 8 wrt tool CS 7

Loc		Loc Err		LSL	USL
X axis rot. (deg)	0	ex (deg)	0	0,000	0,000
Y axis rot. (deg)	0	ey (deg)	0	0,000	0,000
Z axis rot. (deg)	0	ez (deg)	0	0,000	0,000
X axis translation	0	dx	0		
Y axis translation	0	dy	0		
Z axis translation	0	dz	0		

Tool Axis 9 wrt tool CS 8

Loc		Loc Err		LSL	USL
X axis rot. (deg)	0	ex (deg)	0	-1,079	1,079
Y axis rot. (deg)	0	ey (deg)	0	-0,427	0,427
Z axis rot. (deg)	0	ez (deg)	0	-0,887	0,887
axis translation	0	dx	0	-0,201	0,2012
axis translation	-13	dy	0	-0,284	0,2837
axis translation	-27	dz	0	-0,245	0,2449

Work Axis 9 wrt tool CS 8

Loc		Loc Err		LSL	USL
X axis rot. (deg)	0	ex (deg)	0	0,000	0,000
Y axis rot. (deg)	0	ey (deg)	0	0,000	0,000
Z axis rot. (deg)	0	ez (deg)	0	0,000	0,000
X axis translation	0	dx	0		
Y axis translation	0	dy	0		
Z axis translation	0	dz	0		

Tool Axis 10 wrt tool CS 9

Loc		Loc Err		LSL	USL
X axis rot. (deg)	0	ex (deg)	0	-0,093	0,093
Y axis rot. (deg)	0	ey (deg)	0	-1,721	1,721
Z axis rot. (deg)	0	ez (deg)	0	-0,963	0,963
axis translation	-12	dx	0	-0,202	0,2017
axis translation	-221	dy	0	-0,202	0,2017
axis translation	41,5	dz	0	-0,361	0,3606

Work Axis 10 wrt tool CS 9

Loc		Loc Err		LSL	USL
X axis rot. (deg)	0	ex (deg)	0	0,000	0,000
Y axis rot. (deg)	0	ey (deg)	0	0,000	0,000
Z axis rot. (deg)	0	ez (deg)	0	0,000	0,000
X axis translation	0	dx	0		
Y axis translation	0	dy	0		
Z axis translation	0	dz	0		

Tool Axis 11 wrt tool CS 10

Loc		Loc Err		LSL	USL
X axis rot. (deg)	0	ex (deg)	0	-0,026	0,026
Y axis rot. (deg)	0	ey (deg)	0	-0,026	0,026
Z axis rot. (deg)	0	ez (deg)	0	0,000	0,000
axis translation	0	dx	0	-0,025	0,025
axis translation	0	dy	0	-0,025	0,025
axis translation	-55	dz	0	-0,3	0,3

Work Axis 11 wrt tool CS 10

Loc		Loc Err		LSL	USL
X axis rot. (deg)	0	ex (deg)	0	0,000	0,000
Y axis rot. (deg)	0	ey (deg)	0	0,000	0,000
Z axis rot. (deg)	0	ez (deg)	0	0,000	0,000
X axis translation	0	dx	0		
Y axis translation	0	dy	0		
Z axis translation	0	dz	0		

Tool Axis 12 wrt tool CS 11

Loc		Loc Err		LSL	USL
X axis rot. (deg)	0	ex (deg)	0	0,000	0,000
Y axis rot. (deg)	0	ey (deg)	0	0,000	0,000
Z axis rot. (deg)	0	ez (deg)	0	0,000	0,000
axis translation	0	dx	0		
axis translation	0	dy	0		
axis translation	0	dz	0		

Work Axis 12 wrt tool CS 11

Loc		Loc Err		LSL	USL
X axis rot. (deg)	0	ex (deg)	0	0,000	0,000
Y axis rot. (deg)	0	ey (deg)	0	0,000	0,000
Z axis rot. (deg)	0	ez (deg)	0	0,000	0,000
X axis translation	0	dx	0		
Y axis translation	0	dy	0		
Z axis translation	0	dz	0		

Tooltip location in CS 12

Loc in last CS		Loc Err		LSL	USL
Tx	0	dx	0	0	0
Ty	0	dy	0	0	0
Tz	-285	dz	0	-0,5	0,5

Workpiece point of interest in CS 12

Loc in last CS		Loc Err		LSL	USL
Wx5	0	dx	0	-0,152	0,152
Wy5	0	dy	0	-0,152	0,152
Wz5	85	dz	0	-0,574	0,574

OUTPUTS

HTM error between T and W origins in ref CS
Coordinate systems, not tooltip

0,669130606	-0,7431	0	893,091
0,743144825	0,66913	0	70,5047
0	0	1	-312,5
0	0	0	1

HTM: ref T n (position of tool origin not tool tip)
From: rT1*1T2*2T3*3T4*...

0,669130606	0,7431	0	-649,99
-0,743144825	0,6691	0	120,5192
0	0	1	386,5
0	0	0	1

HTM: ref W n (position of workpiece orig
From: rT1*1T2*2T3*3T4*...

1	0	0	0
0	1	0	-496
0	0	1	74,0035
0	0	0	1

Position difference between tool and workpiece in reference coordinates:

d(Tx-Wx)	-649,99	0,00	649,99
d(Ty-Wy)	616,519	0,00	-616,52
d(Tz-Wz)	-57,504	0,18	57,68
	895,87	0,176502	

Tool point coordinates in reference frame:
From: rT1*1T2*2T3*3T4*...*TXYZ

Tx	-649,99	
Ty	120,519	
Tz	101,5	
	1	

Workpiece point coordinates in reference fra
From: rT1*1T2*2T3*3T4*...*TXYZ

Wx	0	
Wy	-496	
Wz	159,0035	
	1	

Appendix 2. X axis sensitivity charts of defined tolerance in drawing

Appendix 3. Y axis sensitivity charts of defined tolerance in drawing

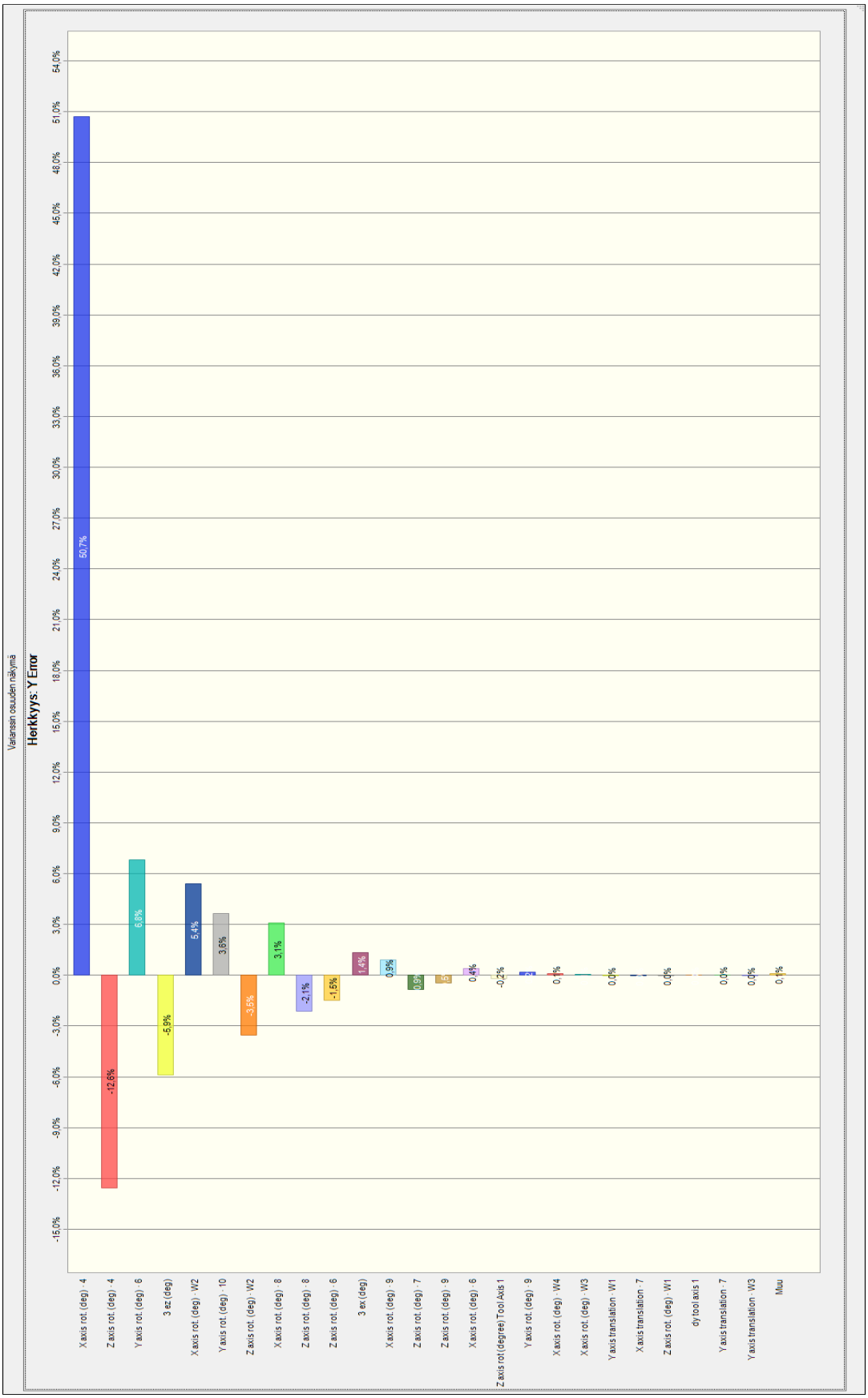

Appendix 4. Z axis sensitivity charts of defined tolerance in drawing

Appendix 5. RMS sensitivity charts of defined tolerance in drawing

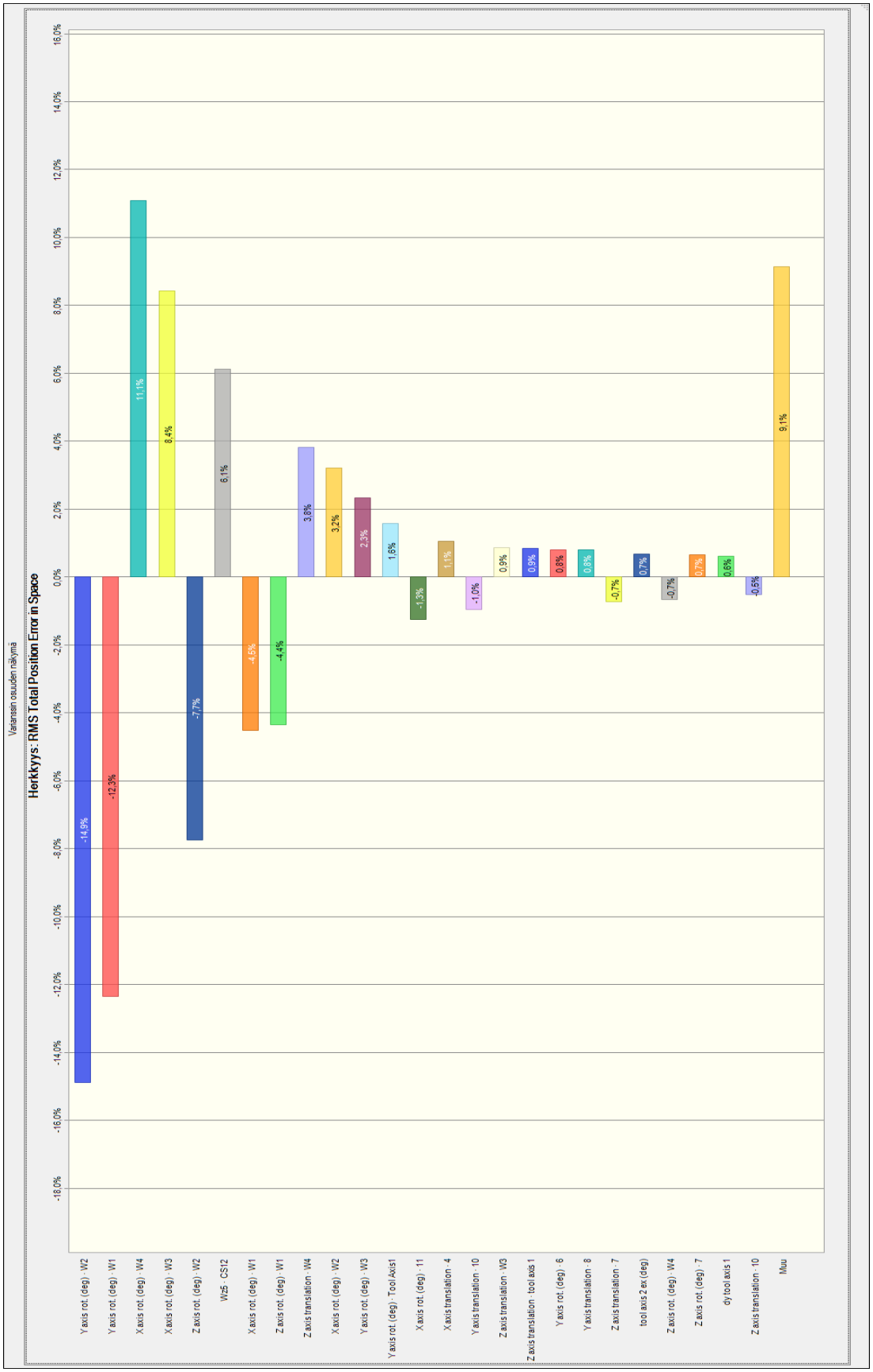

Appendix 6. X axis sensitivity charts of 3D scanning

Appendix 7. Y axis sensitivity charts of 3D scanning

Appendix 8. Z axis sensitivity charts of 3D scanning

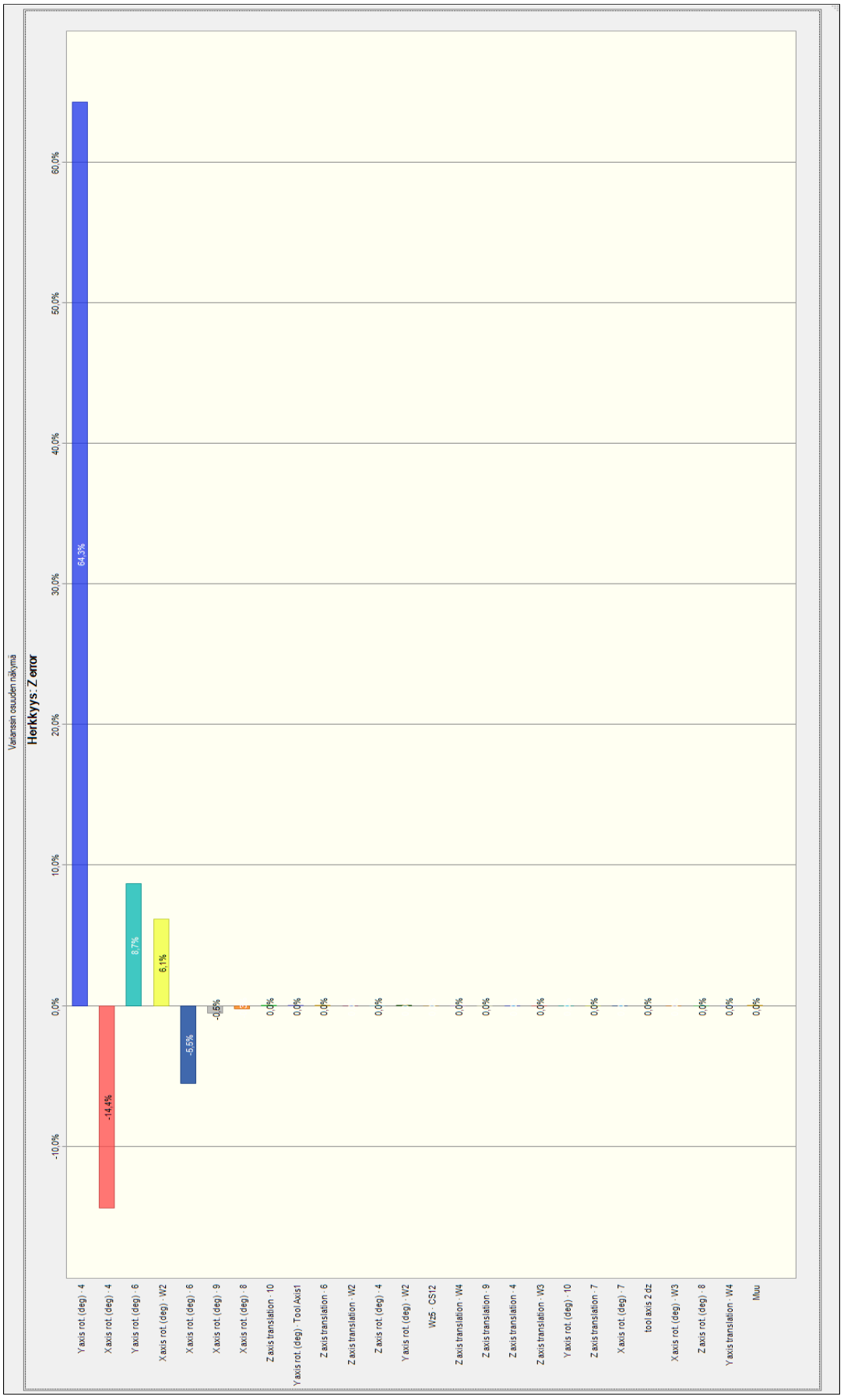

Appendix 9. RMS sensitivity charts of 3D scanning